HHS Public Access

Author manuscript

Brain Behav Immun. Author manuscript; available in PMC 2024 October 01.

Published in final edited form as:

Brain Behav Immun. 2024 October ; 121: 192–210. doi:10.1016/j.bbi.2024.07.010.

Autoimmune inflammation triggers aberrant astrocytic calcium signaling to impair synaptic plasticity

A.M. Baraibar[a,b,c,d,1], **T. Colomer**[a,b,c,1], **A. Moreno-García**[a,b,c], **A. Bernal-Chico**[a,b,c], **E. Sánchez-Martín**[a,b,c], **C. Utrilla**[a,b,c], **R. Serrat**[e,f], **E. Soria-Gómez**[a,b], **A. Rodríguez-Antigüedad**[a,c], **A. Araque**[g], **C. Matute**[a,b,d], **G. Marsicano**[e,f,*], **S. Mato**[a,b,c,*]

[a]Department of Neurosciences, University of the Basque Country UPV/EHU, 48940 Leioa, Spain

[b]Achucarro Basque Center for Neuroscience, 48940 Leioa, Spain

[c]Neuroinmunology Group, Biobizkaia Health Research Institute, 48903 Barakaldo, Spain

[d]Centro de Investigación Biomédica en Red sobre Enfermedades Neurodegenerativas (CIBERNED), 28029 Madrid, Spain

[e]Institut National de la Santé et de la Recherche Médicale (INSERM), U1215 NeuroCentre Magendie, 33077 Bordeaux, France

[f]University of Bordeaux, 33077 Bordeaux, France

[g]Department of Neuroscience, University of Minnesota, Minneapolis, 55455 MN, USA

Abstract

Cortical pathology involving inflammatory and neurodegenerative mechanisms is a hallmark of multiple sclerosis and a correlate of disease progression and cognitive decline. Astrocytes play a pivotal role in multiple sclerosis initiation and progression but astrocyte-neuronal network alterations contributing to gray matter pathology remain undefined. Here we unveil deregulation

*Corresponding authors at: INSERM, U1215 NeuroCentre Magendie, 33077 Bordeaux, France (G. Marsicano). Department of Neurosciences, University of the Basque Country UPV/EHU, 48940 Leioa, Spain (S. Mato). giovanni.marsicano@inserm.fr (G. Marsicano), susana.mato@ehu.eus (S. Mato).

[1]These authors contributed equally: Andrés M Baraibar, Teresa Colomer.

Author contributions

G.M and S.M. conceptualized and supervised the study. A.M.B performed *ex vivo* electrophysiology and imaging experiments. T.C. conducted imaging and expression analyses in astrocyte cultures and purified cells. A.M.-G. and R.S. performed and supervised *in vivo* imaging experiments. T.C., E.S., C.L.U., and A.B.-C. conducted and supervised mouse perfusion and immunohistochemistry experiments. F.S.-L. provided guidance for the analysis of confocal microscopy images. E.S.-G. provided some $CB_1^{f/f}$ mice to the group of S.M. A.R.-A. provided conceptual ideas. A.A. provided data and conceptual support. C.M. performed EAE experiments and provided conceptual support. A.M.B, G.M. and S.M. produced the figures and wrote the paper with input from all authors.

CRediT authorship contribution statement

A.M. Baraibar: Writing – review & editing, Writing – original draft, Visualization, Validation, Investigation, Formal analysis. **T. Colomer:** Visualization, Investigation, Formal analysis. **A. Moreno-García:** Investigation, Formal analysis. **A. Bernal-Chico:** Validation, Supervision, Investigation, Formal analysis. **E. Sánchez:** Investigation, Formal analysis. **C. Utrilla:** Investigation, Formal analysis. **R. Serrat:** Supervision, Investigation, Formal analysis. **E. Soria-Gómez:** Resources. **A. Rodríguez-Antigüedad:** Conceptualization. **A. Araque:** Resources, Conceptualization. **C. Matute:** Investigation. **G. Marsicano:** Writing – review & editing, Writing – original draft, Supervision, Funding acquisition, Conceptualization. **S. Mato:** Writing – review & editing, Writing – original draft, Supervision, Project administration, Funding acquisition, Conceptualization.

Appendix A. Supplementary data

Supplementary data to this article can be found online at https://doi.org/10.1016/j.bbi.2024.07.010.

of astrocytic calcium signaling and astrocyte-to-neuron communication as key pathophysiological mechanisms of cortical dysfunction in the experimental autoimmune encephalomyelitis (EAE) model of multiple sclerosis. Using two-photon imaging *ex vivo* and fiber photometry in freely behaving mice, we found that acute EAE was associated with the emergence of spontaneously hyperactive cortical astrocytes exhibiting dysfunctional responses to cannabinoid, glutamate and purinoreceptor agonists. Abnormal astrocyte signaling by G_i and G_q protein coupled receptors was observed in the inflamed cortex. This was mirrored by treatments with pro-inflammatory factors both *in vitro* and *ex vivo*, suggesting cell-autonomous effects of the cortical neuroinflammatory environment. Finally, deregulated astrocyte calcium activity was associated with an enhancement of glutamatergic gliotransmission and a shift of astrocyte-mediated short-term and long-term plasticity mechanisms towards synaptic potentiation. Overall, our data identify astrocyte-neuronal network dysfunctions as key pathological features of gray matter inflammation in multiple sclerosis and potentially additional neuroimmunological disorders.

Keywords

Astrocyte; Calcium; Gliotransmission; Multiple sclerosis; Cortex

1. Introduction

Multiple sclerosis (MS) is a chronic demyelinating disease of the central nervous system (CNS) initiated by pathogenic immune cell responses against myelin followed by a broader inflammatory and neurodegenerative process (Mahad et al., 2015). Over the last decades a number of neuroimaging and histopathological studies have demonstrated that cortical pathology is centrally involved in MS symptomatology and progression (Calabrese et al., 2010; De Stefano et al., 2003). Functional and structural alterations affecting the cortex are present from the earliest stages of MS, contribute to motor, sensory and cognitive deficits and predict the accumulation of disability (De Stefano et al., 2003; Eshaghi et al., 2018; Feinstein et al., 2014). Neocortical gray matter atrophy in MS involves intermingled inflammatory and neurodegenerative mechanisms that include early excitatory-inhibitory imbalance and widespread synapse loss as key pathological features (Calabrese et al., 2015; Ellwardt et al., 2018; Jafari et al., 2021; Jürgens et al., 2016; Potter et al., 2016). However, the molecular, cellular and circuit mechanisms that drive dysregulated cortical network activity in MS remain unclear.

Astrocytes provide metabolic support and modulate synaptic function and plasticity within neuronal circuits in a broad range of physiological settings. It has long been recognized that astroglial cells respond to synaptically released neurotransmitters with intracellular calcium elevations that culminate in the release of neuroactive substances such as glutamate, adenosine/ATP, D-serine and GABA (Araque et al., 2014). The delivery of these factors termed gliotransmitters enables astrocyte calcium signaling to modulate synaptic strength and fine-tune neuronal network activity in a tightly controlled manner. Astrocytes undergo a pronounced transformation in the context of neuroinflammation whereby they adopt reactive phenotypes and exhibit important disease-promoting functions that contribute to neurological disability (Hasel et al., 2021; Linnerbauer et al., 2020; Patani et al., 2023;

Sofroniew, 2020). Research on the role of reactive astrocytes in MS has established that these cells drive inflammatory lesion formation and promote the neurodegenerative process by multiple mechanisms that include neurotoxicity and dysfunctional astrocyte-to-neuron crosstalk (Chao et al., 2019; Pitt et al., 2000; Ponath et al., 2018). Nevertheless, current understanding on how aberrant interactions between astrocytes and neuronal cells contribute to MS symptomatology and progression, as well as on the role of astrocyte-mediated gliotransmitter release and modulation of synaptic functions during disease neuropathology, remains poor.

Recent advances in functional calcium imaging have led to novel insights on how aberrant astrocytic activity patterns may contribute to neuronal functional deficits in CNS disorders (Shigetomi et al., 2016). Using a combination of imaging approaches applied to the experimental autoimmune encephalomyelitis (EAE) model of MS, we interrogated here how cortical astrocyte calcium dynamics and astrocyte-to-neuron synaptic crosstalk are altered in MS. We show that autoimmune inflammation markedly modifies the intrinsic calcium activity of cortical astrocytes. Notably, these alterations emerge in response to the inflammatory environment and rely on G protein mediated calcium signaling defects. Finally, the dysfunctional astrocyte calcium dynamics encompass aberrant glutamate gliotransmission and deregulation astrocyte-to-neuron plasticity mechanisms towards the potentiation of synaptic excitation. Overall, these data unveil cortical astrocyte-neuron network dysregulation in MS and suggest a novel mechanism of gray matter pathology relying on aberrant astrocyte-dependent modulation of synaptic function during autoimmune inflammation.

2. Methods

2.1. Mice

All experiments were performed in accordance with the Guide for the Care and Use of Laboratory Animals (National Research Council Committee, 2011) and the European Communities Council Directive of September 22th 2010 (2010/63/EU74). Experiments were approved by the local ethical committees of the University of the Basque Country (approval numbers 2017140, M202017144 and 2022245) and the University of Bordeaux (approval number A33063098) and the French Ministry of Agriculture and Forestry (authorization number 3306369). Naive mice on a C57BL/6N background (Janvier, France), IP_3R_2-KO mice (generously donated by Dr. Gertrudis Perea; Instituto Cajal, Madrid, Spain), constitutive CB_1-KO and CB_1-WT mice, $CB_1^{f/f}$ mice (carrying the “floxed” *Cnr1* gene) and inducible GFAP-CB_1-KO mutant mice and GFAP-CB_1-WT littermates (7–14 weeks of age) were used. Cages were enriched and mice were maintained under standard conditions (food and water *ad libitum*; 12 h-12 h light–dark cycle). Experiments were performed during dark cycle (light off at 8:00 h a.m.). EAE was induced in female mice based on epidemiological evidence that MS affects 2–4 times more women than men (Walton et al., 2020). Primary astrocyte cultures were prepared from female and male pups (P4-P5) obtained from homozygote CB_1-WT pairs. The number of mice in each experimental group was similar. No statistical methods were used to predetermine sample size.

GFAP-CB_1-KO mice were generated by crossing $CB_1^{f/f}$ mice (Marsicano et al., 2002) with GFAP-CreERT2 mice (Hirrlinger et al., 2006) using a three-step backcrossing procedure to obtain $CB_1^{f/f;GFAP\text{-}CreERT2}$ and $CB_1^{f/f}$ littermates, called GFAP-CB_1-KO and GFAP-CB_1-WT. Deletion of the *Cnr1* gene was obtained in adult mice (8–9 weeks of age) by daily intraperitoneal (i.p.) injections of tamoxifen (1 mg dissolved at 10 mg/ml in 90 % sesame oil, 10 % ethanol) for 7 days (Han et al., 2012; Robin et al., 2018).

2.2. Drugs

THC was obtained from THC Pharm GmbH (Frankfurt, Germany). ATP disodium salt-hydrate (ATP), thapsigargin and WIN55-212–2 (WIN) were purchased from Sigma-Aldrich (St-Louis, USA); tetrodotoxin (TTX), AM251, clozapine-N-oxide (CNO), (S)DHPG, glutamate monosodium salt-hydrate and LY354740 from Tocris (Bristol, UK). For *in vitro* and *ex vivo* experiments, WIN, AM251 and CNO were dissolved in DMSO; TTX was dissolved in ddH_2O, ATP and LY354740 and glutamate were dissolved in recording media. The concentration of DMSO was never higher than 0.001 %. For *in vivo* administration, THC was prepared freshly before the experiments and was dissolved in a mixture of 5 % ethanol, 4 % cremophor and saline. Doses and concentrations of the different drugs were chosen based on previous published data or preliminary experiments.

2.3. EAE model

Mice were immunized in the flank by subcutaneous (s.c.) injection of 200 μg myelin oligodendrocyte glycoprotein ($MOG_{30\text{-}55}$) peptide (MEVGWYRSPFSRVVHLYRNGK) (Peptide Synthesis Core Facilities of the Pompeu Fabra University, Barcelona, Spain) in incomplete Freund's adjuvant supplemented with 8 mg/ml Mycobacterium tuberculosis H37Ra (Difco Laboratories). Pertussis toxin (500 ng; Calbiochem) was injected i.p. on the day of immunization and again 2 days later. Body weight and motor symptoms were recorded daily and scored from 0 to 8 as follows: 0, no detectable changes in muscle tone and motor behavior; 1, flaccid tail; 2, paralyzed tail; 3, impairment or loss of muscle tone in hindlimbs; 4, hindlimb hemiparalysis; 5, complete hindlimb paralysis; 6, complete hindlimb paralysis and loss of muscle tone in forelimbs; 7, tetraplegia; and 8, moribund.

2.4. Cell culture

Primary astroglial cultures were prepared from homozygote CB_1-WT by magnetic activated cell sorting (MACS). Briefly, the forebrains were carefully dissected, meninges removed and tissue enzymatically dissociated using Neural Tissue Dissociation Kit (P) (Miltenyi Biotec). Myelin was removed using a 35% Percoll PLUS (Merck) gradient and cells were sorted using Anti-ACSA-2^+ MicroBead Kit (Miltenyi Biotec). Cells were seeded onto 14 mm diameter glass coverslips in 24-well plates at a density of 20.000 cells/well for immunocytochemistry and in 6-well plates at a density of 500.000/well for qPCR. Alternatively, astrocytes were seeded onto glass-bottom μ-dishes (Ibidi GmbH) at a density of 100.000 cells/plate for calcium imaging. Cells were maintained in serum-free defined medium containing 50% neurobasal, 50% DMEM, 100 U/mL penicillin, 100 μg/mL streptomycin, 1 mM sodium pyruvate, 292 μg/mL 1-glutamine, 1 × SATO and 5 μg/mL of *N*-acetyl cysteine. This medium was supplemented with the astrocyte-required survival

factor HBEGF (5 ng/mL; Preprotech). The purity of the cultures was be routinely assessed by examining the characteristic cell morphologies under phase-contrast microscopy and confirmed by immunostaining with mouse anti-GFAP (1:200; Merck, MAB3402) and mouse anti-S100β (1:400; Sigma Aldrich, S2532). After 6–7 days in culture $GFAP^+$ and $S100\beta^+$ cells represented 95 ± 1 % and 97 ± 2 % of total cells, respectively ($n = 3$ cultures, 1–2 coverslips per culture, 15 microscopic fields per coverslip). Astrocyte activation to a neurotoxic phenotype was induced in cells at 4–5 DIV by incubation with TNFα (25 ng/mL; Cell Signaling Technology), IL-1α (3 ng/mL; Sigma), and C1q (400 ng/mL; MyBioSource) for 18–24 h and corroborated by immunofluorescence and qPCR analysis (Supplementary Fig. 6).

2.5. Live cell imaging and data analysis

Astrocytes were loaded with Fluo-4 AM (1 mM; Molecular Probes) in culture media for 20 min at 37 °C followed by 10 min wash in Hanks Balanced Salt Solution (HBSS) (Sigma, H-4891) supplemented with (in mM): 20 HEPES, 10 glucose, 2 $CaCl_2$, 1 $MgCl_2$ and 4 $NaHCO_3$ (pH 7.4) to allow de-esterification. Images were acquired through a 63X objective in a TCS SP8X STED CW confocal microscope (Leica) at an acquisition rate of 1 frame/10 s during 5 min. Following a baseline recording (1 min) cells were stimulated with WIN (1 μM), ATP (200 μM), glutamate (200 μM), (S)DHPG (100 μM), LY354740 (100 μM) or thapsigargin (1 μM). Recordings aimed at testing mitochondrial and/or endoplasmic reticulum responses were carried out in the absence of extracellular calcium. For data analysis, a homogeneous population of 10–15 cells was selected in the field of view and regions of interest (ROIs) defined within astrocyte somata. Background values were always subtracted and data are expressed as $\Delta F/F_0$ in which F represents the fluorescence value for a given time point and F_0 represents the mean of the resting fluorescence level.

2.6. Surgery for AAV administration and fiber implantation

Mice (7–8 weeks of age) were anaesthetized with isoflurane and placed on a heating-pad to keep the body temperature at 37 °C. Eye dehydration was prevented by topical application of ophthalmic gel and analgesia was achieved by s.c. injection of buprenorphine (Buprecare, 0.05 mg/kg). The skin above the skull was shaved with a razor and disinfected with modified ethanol 70 % and betadine before an incision was made. Mice were placed into a stereotaxic apparatus (David Kopf Instruments) with mouse adaptor and lateral ear bars.

C57BL6N, IP_3R_2-KO and $CB_1^{f/f}$ mice were injected with AAV5-pZac2.1-gfaABC1d-cyto-GCaMP6f (Addgene), AAV5/2-hGFAP-hM3D (G_q)/hM4D(G_i)_mCherry-WPRE-hGHp(A) (ETH Zurich) alone or in combination with and ssAAV9/2-hGFAP-mCherry_iCre-WPRE-hGHp(A) (ETH Zurich) or ssAAV9/2-hGFAP-mCherry-WPRE-hGHp(A) (ETH Zurich) for *ex vivo* imaging and electrophysiology. Virus v275-9 ssAAV9/2-GFAP-hHBbI/E-GCaMP6f-bGHp(A) was used for fiber photometry imaging of astrocytes in C57BL6N, CB_1-KO and GFAP-CB_1-KO mutant mice and control littermates. Virus titers were between 10^{10} and 10^{12} genomic copies per mL. Stereotaxic injections were targeted to the mouse somatosensory cortex according to the following coordinates (from bregma): anterior-posterior −1.5; medial-lateral ± 2.5; dorsal–ventral −1.5. Viral particles were injected at 400–500 nL alone or in combination at a maximum rate of 100 nL/min using a glass

pipette attached to a Nanojet III (Drummond, Broomall, USA). Following virus delivery, the syringe was left in place for 10 min before being slowly withdrawn from the brain. For fiber photometry experiments, the optical fiber (400 μm diameter) was placed 250 μm above the injection site during the same surgical session. Mice were weighed daily and individuals that failed to return to their pre-surgery body weight were excluded from subsequent experiments. Wild-type, CB_1-WT and CB_1-KO mice and $CB_1^{f/f}$ mice were used for EAE induction 2 weeks after surgery. GFAP-CB_1-KO and GFAP-CB_1-WT mice were treated with tamoxifen 1 week after the surgery and were used for EAE experiments 3 weeks after the last tamoxifen injection.

2.7. Cortical slice preparation for imaging and electrophysiology

Mice were euthanized by decapitation and brains were rapidly removed and placed in ice-cold artificial cerebrospinal fluid (aCSF). Coronal brain slices (350 μM-thick) containing the somatosensory cortex were prepared via a Leica VT1200 vibratome in a 4°C aCSF solution (Baraibar et al., 2023). Following cutting, slices were allowed to recover in aCSF containing (in mM): 124 NaCl, 2.69 KCl, 1.25 KH_2PO_4, 2 $MgSO_4$, 26 $NaHCO_3$, 2 $CaCl_2$ and 10 glucose, gassed with 95% O_2/5%CO_2 (pH=7.3–7.4) at 31°C for 30 min followed by at least 30 min at 20–22°C before recording. Slices were then transferred to an immersion recording chamber and superfused at 2 ml/min with gassed aCSF and the temperature of the bath solution was kept at 34°C with a temperature controller TC-324C (Warner Instruments Co.). EAE mice were processed of *ex vivo* imaging and electrophysiology at 13–21 dpi. Experiments aimed at testing the effects of pro-inflammatory mediators on astrocyte calcium dynamics were performed in slices from naïve mice incubated with TNFα (25 ng/mL), IL-1α (3 ng/mL), and C1q (400 ng/mL) for 30 min immediately before recording.

2.8. Ex vivo two-photon imaging

Two-photon microscopy imaging of layer V-VI astrocytes in the somatosensory cortex was performed using a Femto-2D microscope equipped with a tunable Ti:Sapphire MaiTai DeepSee laser (Spectra Physics) and GaAsP PMT detectors. The laser was tuned at 920 nm with a 20X water immersion lens (1.00 N.A.; Olympus) and a 490/60 nm filter. All calcium experiments were performed in the presence of TTX (1 μM). Videos were obtained at 512 × 512 resolution with a sampling interval of 1 s. Analysis and quantification fluorescence levels in astrocytes was performed with a custom MATLAB program (Calsee: https://www.araquelab.com/code/). Calcium variations recorded at the soma and processes of the cells were estimated as changes of the fluorescence signal over baseline ($\Delta F/F_0$), and cells were considered to show a calcium event when the $\Delta F/F_0$ increase was at least two times the standard deviation of the baseline.

Basal astrocyte calcium activity was quantified from the astrocyte calcium event frequency, which was calculated from the number of events per min within 3 min of recording. Evoked astrocyte calcium activity was quantified from the calcium event probability, which was calculated from the number of calcium elevations grouped in 15 s bins recorded from 8 to 30 astrocytes per field of view. The time of occurrence was considered at the onset of the calcium event. For each astrocyte analyzed, values of 0 and 1 were assigned for bins showing either no response or a calcium event, respectively, and the calcium event

probability was obtained by dividing the number of astrocytes showing an event at each time bin by the total number of monitored astrocytes (Navarrete and Araque, 2010). All the astrocytes that showed a calcium event during the experiment were used for the analysis. The calcium event probability was calculated in each slice, and for statistical analysis, the sample size corresponded to the number of slices. To examine the difference in calcium event probability in distinct conditions, the basal calcium event probability (mean of the 1 min before a stimulus) was averaged and compared to the average calcium event probability (15 s after a stimulus). For drug application, a micropipette was filled with WIN (300 μM), glutamate (200 μM), ATP (200 μM), (S) DHPG (100 μM), LY354740 (100 μM) or CNO (1 mM) solution and placed 100–150 μm away from the tissue and a pressure pulse at 1 bar was applied for 5 s. The effect of the CB_1 antagonist AM251 (2 μM) was tested after 10 min bath perfusion in the same region and same astrocytes recorded in control conditions.

2.9. Electrophysiology

Electrophysiological recordings from layer V pyramidal neurons were made using the whole-cell-patch-clamp technique (Baraibar et al., 2023). Cells were visualized using infrared-differential interference contrast optics (Olympus BX51WI microscope, Olympus Optical, Japan) and 40X water immersion lens and selected for recording based on their location, morphology, and firing pattern. When filled with an internal solution containing (in mM): 110 potassium gluconate, 40 HEPES, 4 NaCl, 4 ATP-Mg, and 0.3 GTP (pH = 7.3) patch electrodes exhibited a resistance of 3–10 MΩ. All recordings will be performed using Multi-Clamp 700B amplifier (Molecular Devices, San Jose, CA). Fast and slow whole-cell capacitances were neutralized, and series resistance was compensated (~70%), and the membrane potential was held at −70 mV. Intrinsic electrophysiological properties were monitored at the beginning and the end of the experiments. Series and input resistances were monitored throughout the experiment using a −5 mV pulse. Recordings were considered stable when the series and input resistances, resting membrane, and stimulus artifact duration did not change > 20%. Signals were fed to a Pentium-based PC through a DigiData 1550 interface board. Signals were filtered at 1 KHz and acquired at a 10 KHz sampling rate using a DigiData 1550 data acquisition system and pCLAMP 10.3 software (Molecular Devices, San Jose, CA). Theta capillaries (2–5 μm tip) filled with ACSF were used for bipolar stimulation and placed in layer 2/3. Electrical pulses were supplied by a stimulus isolation unit (ISO-Flex, A.M.P.I, Jerusalem, Israel). Excitatory postsynaptic currents (EPSCs) were induced using brief current pulses (1 ms) delivered at 0.33 Hz and isolated using picrotoxin (50 μM) and CGP5462 (1 μM) to block $GABA_A$ and $GABA_B$ receptors, respectively. EPSC amplitude was determined as the peak current amplitude (2–20 ms after stimulus) minus the mean baseline current (10–30 ms before stimulus).

Input-output curves of EPSCs were obtained by increasing stimulus intensities from 0 to 100 μA in 10 μA steps. Paired-pulse facilitation was analyzed by applying paired pulses with 25, 50, 75, 100, 150, 200, 300 and 500 ms inter-pulse intervals. The paired-pulse ratio was calculated by dividing the amplitude of the second EPSC by the first (PPR = EPSC-2/EPSC-1). Synaptic fatigue was assessed by applying 19 consecutive stimuli in 25 ms intervals. AMPA and NMDA currents were obtained with an internal solution containing (in mM): 117 cesium gluconate, 20 HEPES, 0.4 EGTA, 2.8 NaCl, 5 TEA-Cl, 2 ATP and 0.3

GTP. AMPA currents were obtained at a holding potential of −70 mV and NMDA currents at +30 mV. To ascertain the AMPA to NMDA receptor current ratio, we measured the NMDA component 50 ms after the stimulus.

For paired recordings, neurons were selected following the same vertical axis and distance of the somas of the layer V paired-recorded neurons varied from 70 to 270 μm. To induce endocannabinoid-mediated short-term synaptic plasticity pyramidal neurons were depolarized from −70 mV to 0 mV for 5 s (ND). Synaptic parameters were determined from 40 stimuli before (basal) and following ND. Baseline mean EPSC amplitude was obtained by averaging mean values calculated within 2 min of baseline recordings and mean EPSC amplitudes were normalized to baseline. The ND was applied 2.5 s after the last basal delivered pulse and no pulses were presented during the ND. The 0.33-Hz pulse protocol was restarted immediately after the ND step. To illustrate the time course of ND-induced effects, synaptic parameters were grouped in 30 s bins. Two consecutive responses to ND were averaged. For every synaptic recording, the presence of heteroneuronal depression or potentiation was assessed in individual synaptic recordings if the EPSC amplitude decreased or increased > 2 times the standard deviation of the baseline EPSC amplitude during the first 45 s after the ND.

To induce spike-timing dependent plasticity (STDP) layer V pyramidal neurons were kept in voltage-clamp mode before and after the pairing protocol and EPSCs evoked by stimulation in layer II-III at 0.33-Hz. During the pairing protocol neurons were kept in current clamp mode and EPSPs were paired with one postsynaptic action potential at a time interval of $\Delta t = -25$ ms and pairings were repeated 60 times at 0.1 Hz (Min and Nevian, 2012). Experiments were discarded if the pyramidal neuron input resistance changed by > 20 % during the course of the experiment.

Miniature excitatory postsynaptic currents (mEPSCs) and slow inward currents (SICs) mediated by astrocytic glutamate release (Fellin et al., 2004; Perea and Araque, 2005; Pirttimaki et al., 2017) were isolated in the presence of tetrodotoxin (TTX, 1 μM), picrotoxin (50 μM) and CGP54626 (1 μM) to block voltage-gated Na^+ channels, $GABA_A$, and $GABA_B$ receptors, respectively. In all cases the effects of pharmacological agents were tested after 10 min bath perfusion and at < 40 min after entering whole-cell mode in the stimulating neuron.

2.10. Fiber photometry imaging

Freely moving mice were imaged using 470 and 405 nm LEDs to excite GCaMP6s after 3 days of handling habituation. The emitted fluorescence is proportional to the calcium concentration for stimulation at 470 nm (Akerboom et al., 2013; Ohkura et al., 2012). The isosbestic 405 nm stimulation (UV light) was used in alternation with the blue light (470 nm) for analysis purposes as the fluorescence emitted after this stimulation is not depending on calcium (Lütcke et al., 2010). The GCaMP6s fluorescence from the astrocytes was collected with a sCMOS camera through an optic fiber divided in 2 sections: a short fiber implanted in the brain of the mouse and a long fiber (modified patchcord), both connected through a ferrule-ferrule (1.25 mm) connection. MATLAB program (Matlabworks) was used to synchronize each image recording made by the camera, and the Mito-GCaMP6s light excitation made by the LEDs (470 and 405 nm). The two wavelengths of 470 and 405 nm

at a power of 0.1 mW were alternated at a frequency of 20 Hz each (40 Hz alternated light stimulations).

To calculate fluorescence due specifically to calcium fluctuations and to remove bleaching and movement artifacts, the isosbestic 405 nm signal was subtracted from the 470 nm calcium signal. Specifically, normalized fluorescence changes ($\Delta F/F_0$) were calculated by subtracting the mean fluorescence (2 min sliding window average) from the fluorescence recorded by the fiber at each time point and dividing this value by the mean fluorescence ($(F-F_{mean})/F_{mean}$) using a customized Matlab software. Subsequently, the calcium independent isosbestic signal was subtracted to the raw signal emitted after the 470 nm excitation to eliminate unspecific fluorescence. The result will be the global calcium signal ($\Delta F/F$ (%) = $\Delta F_{Ca} – \Delta F_{isos}$), that was used as an estimate of tonic activity of the astrocytes. Calcium transients were detected on the filtered trace (high filter) using a threshold to identify them (2 median absolute deviation –MAD– of the entire trace). Duration and frequency were calculated on the detected transients. Amplitude was determined as the MAD of each studied period. The effects of vehicle and THC injection were analyzed in 2 equal time periods after injection (*period 1* and *period 2*) (Serrat et al., 2021).

The day of recording each mouse was placed in a rectangular chamber and its behavior recorded using a camera placed above the chamber. In experiments aimed at evaluating the effect of THC in naïve mice, baseline recordings were made for 15 min. Animals were subsequently injected i.p. with vehicle solution and recorded for further 30 min after injection (15 min *period 1* + 15 min *period 2*). Mice were returned to the home cage following vehicle recordings. At least 24 h after vehicle recordings mice were injected with THC solution (10 mg/Kg; i.p.) following a 15 min baseline recording period and imaged for the same time-windows. In experiments designed to address changes in astrocytic calcium responses to THC during autoimmune demyelination EAE was induced following the habituation period. Mice were injected with vehicle and THC (10 mg/Kg; i.p.) at 20–21 dpi and recordings made as described above.

2.11. Flow cytometry

Mice were decapitated under isoflurane anesthesia (IsoVet®, B Braun) and cells purified from the forebrain according to previously described procedures (Moreno-García et al., 2020). Briefly, tissue was dissected and placed in enzymatic solution containing (in mM): 116 NaCl, 5.4 KCl, 26 $NaHCO_3$, 1 NaH_2PO_4, 1.5 $CaCl_2$, 1 $MgSO_4$, 0.5 EDTA, 25 glucose, 1 L-cysteine with papain (3 U/mL) and DNAse I (150 U/μL, Invitrogen) for digestion during 25 min at 37°C. Halfway through the incubation, the minced tissue was triturated 10 times using 5 mL serological pipettes. Following enzymatic digestion, cells were mechanically released by gentle passage through 23 G, 25 G and 27 G syringe needles. After homogenization, tissue clogs were removed by filtering the cell suspension through prewetted 40 μm cell strainers (Fisherbrand™) to a 50 mL Falcon tube quenched by 5 mL of 20% heat inactivated fetal bovine serum in HBSS (Thermo Fisher Scientific). The cell strainers were thoroughly rinsed with 15 mL HBSS in and cell suspensions were centrifuged 200 x *g* for 5 min. To purify astrocytes from myelin debris, cells were resuspended in

25% isotonic Percoll PLUS (GE Healthcare Europe GmbH) in HBSS and centrifuged at 200 x *g* without brake for 20 min at room temperature (RT). The myelin top layer was aspirated and cells washed with HBSS to remove any traces of Percoll PLUS by centrifuging at 200 x *g* for 5 min. The total dissociated single cells were resuspended in 500 μL sorting buffer (25 mM HEPES, 5 mM EDTA, 1 % BSA, in HBSS) containing Normal Rat Serum (1:100; Invitrogen, 10710C) and TruStain FcX™ (anti-mouse CD16/32) antibody (1:100; BioLegend, 101320). Isolated cells were incubated with fluorochrome conjugated antibodies ACSA-2-PE (1:50; Miltenyi Biotec, REA969), A2B5-488 (1:100; R&D Systems, FAB1416G), CD11b-FITC (1:200; BioLegend, 101205), CD31-VioBright 515 (1:200; Miltenyi Biotec, REA784), CD45-FITC (1:200; Miltenyi Biotec, REA737), O1-488 (1:100; R&D Systems, FAB1327G) and LIVE/DEAD Fixable Green Dead Cell (1:1500; Thermo Fisher, L34969). Samples were run on a BD FACS Jazz (2B/4YG) flow cytometer (BD Bioscience) controlled using BD FACS™ Software (version 1.1.0.84) and results were analyzed using FlowJo software. All gatings were set based on appropriate isotype controls. Debris and cell clumps were initially gated out on the basis of FSC and SSC plots, allowing selection of only the population of interest. Further doublets were gated out using FSC/trigger pulse width plots. Astrocytes were sorted as ACSA-2$^+$ cells following exclusion of contaminating microglia, hematopoietic cells, oligodendrocytes, oligodendrocyte progenitors and endothelial cells grouped in a dump channel. Typically, an average number of 50.000 astrocytes were collected for each sample within 15–20 min. The purity of astrocytes was assessed by flow cytometry analysis of sorted ACSA-2$^+$ cells following fixation and immunostaining with a C-terminal antibody against the astrocytic marker GLAST (Rothstein et al., 1994) (1:200; kindly donated by JD Rothstein). We further confirmed that we had isolated a relatively pure population of astrocytes and microglia by qPCR analysis for the expression of several cell-type specific markers (Moreno-García et al., 2020).

2.12. Quantitative RT-PCR

Anesthetized mice were transcardially perfused with cold phosphate buffer saline (PBS) for 30 s in order to remove blood cells from the brain. The somatosensory cortex was dissected from a single coronal slice trimmed between levels 1 and – 1 bregma. Astrocytes purified by flow cytometry and cultured cells were collected in lysis buffer (Qiagen) containing 1% β-mercaptoethanol for optimal template preservation. Total RNA from brain samples, purified astrocytes and cultured cells was purified with on-column DNAse treatment using RNeasy Plus Micro and Mini kits (Qiagen) following manufacturer's instructions. RNA was eluted with 14–35 μL of RNAse-free deionized water and stored at −80 °C until analysis. Synthesis of cDNA, pre-amplification and amplification steps were performed at the Genome Analysis Platform of the UPV/EHU following quality control of RNA samples with an Agilent 2100 Bioanalyzer (Agilent Technologies). Pre-amplified cDNA samples were measured with no reverse transcriptase and no template controls in the BioMark HD Real-Time PCR System using 48.48 Dynamic Arrays of integrated fluidic circuits (Fluidigm Corporation). We used commercial primers from IDT Integrated DNA Technologies or Fluidigm Corporation (Supplementary Table 1). Data pre-processing and analysis were completed using Fluidigm Melting Curve Analysis Software 1.1.0 and Real-time PCR Analysis Software 2.1.1 (Fluidigm Corporation) to determine valid PCR reactions.

Gapdh, *Hprt*, *Ppia* and *B2m* were included as candidate reference genes for normalization purposes. Data were corrected for differences in input RNA using the geometric mean of reference genes selected according to results from the normalization algorithms geNorm (https://genorm.cmgg.be/) and Normfinder (https://moma.dk/normfinder-software). Relative expression values were calculated with the $2^{-\Delta\Delta Ct}$ method.

2.13. Western blot

Anesthetized mice were transcardially perfused with cold PBS and the somatosensory cortex was dissected from a single coronal slice between levels 1 and – 1 bregma. Cortical tissue was homogenized (1:20 w/v) in ice-cold RIPA buffer (Thermo Scientific™; 89900) containing a protease inhibitor cocktail (Thermo Scientific™; 87786) by using a Potter homogenizer provided with a loosely fitting Teflon pestle. Samples were incubated in ice for 30 min and subjected to centrifugation (12000 x g at 4°C for 8 min) to remove insoluble material. Solubilized proteins were quantified in the supernatants using the BioRad Protein Assay Kit (Protein Assay Reagents; 5000–114-13–15). Protein samples (4 μg) were loaded into polyacrylamide Criterion TGX Precast (BioRad) gels before electrophoretic transfer onto Nitrocellulose membranes (Amersham™ Protran® Western blotting membranes, pore size 0.2 μm). Membranes were blocked for 1 h in Tris-buffered saline (TBS) containing (in mM): 50 Tris and 200 NaCl (pH 7.4) with 0.05% Tween-20 and 5% BSA. Subsequently, membranes were incubated overnight at 4 °C with primary antibodies raised against myelin basic protein (MBP; 1:1000; BioLegend, 808401), myelin oligodendrocyte glycoprotein (MOG; 1:1000; Santa Cruz Biotechnologies, sc-166172), myelin-associated glycoprotein (MAG; 1:1000; Santa Cruz Biotechnologies, sc-376145) and anti-α-tubulin (1:5000; Abcam, ab7291). Membranes were incubated with horseradish peroxidase-conjugated secondary antibodies (1:5000; Cell Signaling Technology) for 1 h at RT and developed with NZY Standard ECL Western Blotting Substrate (NZYtech). Volumetric analysis of relevant immunoreactive bands was carried out after acquisition on a ChemiDoc XRS System (Bio-Rad) controlled by The Quantity One software v 4.6.3 (BioRad).

2.14. Fluorescence immunohistochemistry

Mice were anesthetized with chloral hydrate (400 mg/Kg) and transcardially perfused with 0.9% NaCl followed by 4 % paraformaldehyde dissolved in 0.1 M phosphate buffer (PB) containing (in mM): 25 $NaH_2PO_4{\cdot}H_2O$ and 75 Na_2HPO_4 (pH 7.4). After extraction, the brains were incubated for 3 h in the same fixative and stored in PB at 4 °C. Serial brain coronal sections between bregma −0.95 and −1.91 levels were cut at 40 μm and collected in PB at RT and stored in PB containing 0.02% sodium azide at 4°C until use.

For immunohistochemistry, floating sections were washed three times in TBS containing (in mM): 100 Tris Base and 150 NaCl (pH 7.4) for 10 min and incubated in a blocking-permeabilization solution containing 5% normal goat serum (NGS) and 0.2% Triton X-100 in TBS for 60 min at RT. Sections were subsequently incubated with the corresponding primary antibodies diluted in TBS supplemented with 1% NGS and 0.1% Triton X-100 for 24–72 h at 4°C. The following primary antibodies were used: chicken anti-GFAP (1:500; Abcam, Ab4674), mouse anti-S100b (1:200; Sigma, S2532), rabbit anti-C3d Complement

(1:1000; Dako, A0063), rabbit anti-Iba1 (1:500; Wako, 019–19741), rat anti-CD68 (1:100; Bio-Rad, MCA1957GA), mouse anti-MBP (1:1000; Biolegend, 808402), mouse anti-Olig2 (1:500; Millipore, MABN50), rabbit anti-NG2 (1:500; Millipore, AB5320), mouse anti-APC/CC1 (1:500; Millipore, OP80), mouse anti-Synaptophysin (1:1000; BioLegend, 837101), rabbit anti-Homer-1 (1:500; Synaptic Systems, 160003) and rat anti-CD3 (1:50; Bio-Rad, MCA772). Tissue samples run in parallel without primary antibodies were always included as internal controls. Sections were washed three times in TBS for 10 min each before incubation for 1–2 h at RT with the following Alexa Fluor secondary antibodies made in goat (1:500; Invitrogen): anti-rabbit Alexa 488 (A11008), anti-rabbit Alexa 647 (A21244), anti-chicken Alexa 647 (A21449), anti-rat Alexa 488 (A11006), anti-mouse Alexa 488 (A11001), anti-mouse Alexa 594 (A11005), anti-mouse Alexa 647 (A21235), anti-mouse IgG2a Alexa 594 (A21135), anti-mouse IgG2b Alexa 488 (A21141). Hoechst 33258 (5 μg/mL; Sigma-Aldrich, 861405) was used together with secondary antibodies for chromatin staining. Finally, sections were washed three times for 10 min in TBS, mounted, dried and a coverslip was added on top with ProLong Gold antifade reagent (Invitrogen by ThermoFisher, P36930).

For the analysis of GCaMP6f localization in the mouse somatosensory cortex sections were washed three times for 5 min in PBS (0.1 M, pH 7.4) and incubated with rabbit anti-GFP (1:500; Invitrogen, A11122), chicken anti-GFAP (1:500; Abcam, ab4674) and mouse anti-NeuN (1:500; Millipore, MAB377) overnight at 4°C in a blocking solution containing 10% donkey serum and 0.3% Triton X-100 in PBS. The sections were then washed in PBS for 30 min at RT and primary antibodies were detected by incubation with donkey anti-rabbit Alexa 488 (1:500; Invitrogen, A-21206), donkey anti-chicken Alexa 647 (1:500; Invitrogen, A-78952) and donkey anti-mouse Alexa 594 (1:500; Invitrogen, A-21203) for 2 h at RT. Then, sections were washed for 15 min in PBS, mounted, dried and mounted on microscope slides in Fluoromount G.

Optical images from tissue sections processed in parallel were acquired in the same session using a 20X, 40X or 63X oil immersion lens on a Zeiss Axioplan 2 pseudoconfocal microscope and a Leica TCS STED CW SP8 super-resolution microscope. Image acquisition was carried out using fluorescence intensity settings at which the control sections without primary antibody gave no signal. Immunolabeling was examined bilaterally in layers V-VI of the somatosensory cortex and the CA1 area of the hippocampus using open source image analysis software Fiji Image J (Schindelin et al., 2012). Olig2, CC1 and NG2 immunopositive cells were counted in a selected ROI using a cell counter plugin and data expressed as mean cell number per square millimeter (mm^2) of tissue area. Analysis of immunostained areas and synaptic particles was performed in 16-bit gray scale transformed pictures. MBP, Iba-1, GFAP and C3 signals were considered positive if they were above a defined intensity threshold and normalized to total selected ROI area. For the analysis of Iba1 and CD68 colocalization the overlapping area was calculated from the merged binary images and normalized to Iba-1 stained area. Analysis of GFAP and C3 colocalization was performed using an open-source script (https://github.com/SoriaFN/Tools/blob/master/Autosegment_Coloc.ijm) for Fiji Image J. Synaptic markers were quantified in thresholded images converted to masks. Homer-1 and Synaptophysin immunopositive particles were filtered for a minimum size of 3 pixels, automatically counted and normalized to the ROI

area expressed in μm^2. To evaluate putative synaptic contacts, the mask corresponding to the Homer-1 channel was dilated and the number of overlapping contacts to neighboring objects quantified and normalized to the tissue ROI area in μm^2. Immunohistochemistry data were averaged over 2 images per animal for each staining.

2.15. Statistical analyses

Summary results are presented as mean of independent data points ± SEM that represent the number of animals, slices, neurons or cultures tested. Datasets were initially tested for normal distribution and statistical analysis of the differences between groups were determined by two-tailed unpaired or paired Student *t* test, Mann-Whitney test, one-way ANOVA or two-way ANOVA followed by Šídák's test for multiple comparisons. Differences were considered to be significantly different when $P < 0.05$. Correlation analysis was performed by Pearson's or Spearmans test.

3. Results

3.1. Emergence of aberrant astrocyte calcium responses during EAE

To study the calcium activity of astrocytes during cortical MS pathology we used *ex vivo* two-photon imaging of GCaMP6f in acute slices. As experimental model of MS we induced chronic EAE by immunization with MOG_{35-55} and monitored astrocytes in the somatosensory cortex around the peak of acute disease (13–20 dpi) (Fig. 1a, b). Histological analysis of *postmortem* tissues showed specific expression of the calcium sensor in astrocytes from control and EAE mice (Supplementary Fig. 1).

We first addressed possible EAE-induced changes in naturally occurring calcium fluctuations, which reflect the integration of both activity-dependent and -independent cellular signals (Wang et al., 2006; Zur Nieden and Deitmer, 2006). Experiments were performed in the presence of TTX to record activity-independent calcium dynamics in astrocytes and thus exclude potential confounding effects from altered cortical excitatory-inhibitory balance associated with EAE pathology (Potter et al., 2016). Under these experimental conditions, astrocytes within layer V-VI of the somatosensory cortex exhibited sparse spontaneous calcium activity in control conditions (Fig. 1c, d). We observed a 2-fold increase in the calcium event probability of cortical astrocytes at acute EAE disease (Fig. 1c-e; Supplementary videos S1 and S2). In addition, immunized mice displayed astrocyte calcium events of drastically enhanced duration (Fig. 1f; Supplementary videos S3 and S4) and slightly larger amplitude (Fig. 1g). Collectively, these results suggest that astrocytes of the somatosensory cortex display spontaneous calcium hyperactivity during EAE.

3.2. EAE impairs CB_1 receptor-mediated astrocyte calcium responses

A prominent mechanism by which cortical astrocytes communicate with their environment is endocannabinoid signaling, which evokes intracellular calcium elevations through astrocyte CB_1 receptors *ex vivo* and *in vivo* (Baraibar et al., 2023; Min and Nevian, 2012; Serrat et al., 2021). Changes in the levels of endocannabinoid ligands and receptor proteins have been pinpointed in human MS (Eljaschewitsch et al., 2006) and animal models of the disease (Baker et al., 2001; Centonze et al., 2007; Moreno-García et al., 2020),

prompting us to explore potential alterations in astrocyte calcium responses evoked by CB_1 receptors during EAE. To address this issue, we first performed fiber photometry imaging of astrocytic GCaMP6f in naïve, freely behaving mice treated with the plant-derived cannabinoid compound Δ^9-tetra-hydrocannabinol (THC, 10 mg/Kg) (Supplementary Fig. 2a). Time-course image analysis revealed that THC treatment increased the amplitude and duration of astroglial calcium signals in the somatosensory cortex of naïve CB_1-WT mice, but not in CB_1-KO mice (Supplementary Fig. 2b-d). This results is consistent with our recent observation that *in vivo* activation of CB_1 receptors increases the occurrence of mitochondrial calcium events in cortical astrocytes (Serrat et al., 2021). We next used conditional mutant mice lacking CB_1 receptors in GFAP-positive cells (GFAP-CB_1-KO mice) (Han et al., 2012) to decipher whether the increase of astrocyte cytosolic calcium activity induced by THC was due to a direct activation of CB_1 receptors in astroglial cells. Systemic THC did not modulate the dynamics of astroglial calcium events in the somatosensory cortex of GFAP-CB_1-KO mice while reliably increased the amplitude of calcium signals in control littermates (GFAP-CB_1-WT) recorded in parallel (Supplementary Fig. 2f-g). Thus, THC increases astrocyte calcium activity in the somatosensory cortex of freely-behaving mice through the activation of CB_1 receptor populations present in astroglial cells.

Next, we explored whether the observed changes in the activity patterns of astrocytic calcium responses during EAE involved deficient regulation of cytosolic calcium levels by CB_1 receptors. Mice subjected to EAE were sequentially challenged with vehicle and THC at established disease in 2 consecutive sessions separated 24 h (20–21 dpi) (Fig. 2a, b). Mirroring results in naïve CB_1-WT mice (Supplementary Fig. 2b-d), systemically administered THC effectively increased the amplitude and duration of astroglial calcium transients during the second half of the recordings in control non-immunized mice (Fig. 2c-e). Noteworthily, injection of THC did not modulate the *in vivo* calcium dynamics of cortical astrocytes in EAE mice during the recording session (Fig. 2c-e) suggesting deficits in astrocyte CB_1 receptor-mediated activity. To further corroborate this hypothesis, we monitored calcium responses to the cannabinoid agonist WIN55,212-2 (WIN, 300 μM) in cortical astrocytes of EAE mice using *ex vivo* two-photon microscopy in acute slices (Fig. 3a). While local application of WIN increased spontaneous astrocyte calcium activity in naïve mice, WIN-evoked responses were significantly reduced in EAE mice (Fig. 3b-d; Supplementary videos S5 and S6). Thus, EAE is associated with an impaired ability of CB_1 receptors to modulate cytosolic calcium activity in cortical astrocytes.

3.3. Cell autonomous deregulation of astrocyte calcium dynamics involves deficits in G_i and G_q signaling pathways

Aberrant calcium responses of cortical astrocytes during EAE may be cell autonomous and/or reflect disease-associated changes in the dynamics of extracellular signals coupled to the modulation of calcium dynamics in these cells (i.e. endocannabinoids, glutamate or ATP/adenosine). Of note, astrocytes activated during EAE display reduced gene expression levels of CB_1 receptors (Moreno-García et al., 2020), which provides a plausible cell autonomous mechanism underlying the observed deficits in calcium responses to cannabinoid agonists *ex vivo* and *in vivo*. Thus, we next asked whether reorganization of astrocyte calcium

signaling during EAE involves abnormal expression of additional membrane receptors and calcium handling molecular cascades using RT-qPCR. Astrocytes purified from mice at acute EAE disease showed deregulated transcript levels of several calcium handling signaling/homeostatic toolkits (Fig. 3e). Among the genes whose expression were altered, we found complex changes in several receptors mediating glutamate signaling to astrocytes, such as metabotropic glutamate receptors (mGluRs) type 1 (*Grm1*), 3 (*Grm3*) and 5 (*Grm5*) (Haustein et al., 2014; Sun et al., 2013) as well as decreased levels of several adenosine receptors (*Adora2a*, *Adora2b*). Our RT-qPCR analysis also showed reductions in the expression levels of molecules chiefly involved the regulation of astrocytic calcium responses by the endoplasmic reticulum and the mitochondria, namely the IP_3R_2 (*Itpr2*) and the mitochondrial calcium uniporter (*Mcu*). Altogether, these results suggest that astrocytes at acute EAE disease display widespread deficits in calcium signaling pathways that are essential for their physiological functions.

To decipher whether deficits in astrocyte CB_1 receptor-mediated calcium responses extend to signaling by additional neurotransmitter receptors we conducted two-photon imaging experiments in acute cortical slices from EAE mice. Calcium signals evoked by locally applied ATP and glutamate (200 μM) were significantly reduced at acute EAE disease thus mirroring impaired responses to the cannabinoid agonist WIN (Fig. 3f). We also found significantly reduced calcium responses to the $mGluR_{2/3}$ agonist LY354740 (100 μM; Fig. 3f) which are consistent with the deficits in astrocyte *Grm3* expression during EAE determined by qPCR (Fig. 3e). Noteworthily, calcium signals evoked by the $mGluR_{1/5}$ agonist (S)DHPG (100 μM) in cortical astrocytes were also slightly decreased (Fig. 3f) despite the augmented gene expression levels of both receptor proteins in cells purified from EAE mice (Fig. 3e). These combined results support the possibility that reorganization of astrocyte calcium signaling in the EAE cortex involves differential deficits in the intracellular pathways operated by G_i and G_q proteins in addition to deregulated expression of G protein-coupled receptors. To test this hypothesis, we next investigated the functional consequences of selective activation of G_i and G_q signaling on astrocytic calcium activity using designer receptors exclusively activated by designed drugs (DREADDs) (Roth, 2016). Astrocytes in the somatosensory cortex were specifically targeted with AAV5-GFAP-G_i-DREADD-mCherry or AAV5-GFAP-G_q-DREADD-mCherry in combination with AAV5-gfaABC1d-GCaMP6f and challenged with clozapine-N-oxide (CNO; 1 mM) during acute EAE (Fig. 3g). We found that application of CNO transiently elevated calcium levels in the soma and processes of cortical astrocytes expressing G_i- or G_q-DREADDs as quantitatively shown by the increase of the calcium event probability in naïve mice (Fig. 3h-i). These results confirm and extend previous observations on the ability of both G protein-mediated signaling pathways to activate astroglial cells in terms of calcium dynamics (Baraibar et al., 2023; Durkee et al., 2019; Jiang et al., 2016). EAE induction completely abolished calcium responses induced by CNO in astrocytes expressing G_i-DREADDs (Fig. 3h-i). Responses to CNO were also significantly reduced, albeit to a lower extent, in astrocytes from EAE mice expressing G_q-DREADDs as compared to non-immunized animals (Fig. 3i). The G_i to G_q calcium signaling ratio calculated from the acute increase in calcium event probability following DREADDs activation was decreased by > 2-fold during EAE (control G_i/G_q: 74%; EAE G_i/G_q: 28%). These results provide evidence that cortical astrocytes exhibit

disbalanced calcium responses mediated by G_i and G_q protein signaling pathways that may underlie, at least in part, abnormal calcium dynamics during EAE.

3.4. Cortical pathology involves demyelination, inflammation and astrocyte reactivity

Cortical pathology in MS is characterized by inflammation dominated by innate immune cells, demyelination and a variable extent of synapse loss and neuronal death (Lagumersindez-Denis et al., 2017; Mahad et al., 2015). Previous studies have highlighted that the emergence of synaptic abnormalities in EAE mouse cortex precedes the onset of local inflammatory responses (Yang et al., 2013) but the features of cortical neuropathology in this model of MS remain incompletely defined. Thus, to gain further insight into the cellular and molecular mechanisms that encompass aberrant astrocyte calcium signaling during EAE we next examined cortical demyelination, synaptic dysfunction and inflammation in the acute phase of the disease. Gene and protein expression analysis in cortical lysates showed slight reductions in the levels of the myelin components MBP, MOG and/or MAG in mice at acute EAE disease (Supplementary Fig. 3a-b). Immunofluorescence staining for MBP corroborated that EAE mice display significant demyelination of the somatosensory cortex (Supplementary Fig. 3c-e) and the hippocampus at 17 dpi (Supplementary Fig. 3c, i) consistent with previous observations in this rodent model of MS (Errede et al., 2012; Girolamo et al., 2011; Ziehn et al., 2010). We then immunostained for Olig2 to mark the oligodendrocyte lineage, in combination with CC1 or NG2 to identify myelinating oligodendrocytes or oligodendrocyte precursor cells, respectively. We observed a decline in the presence of $Olig2^+$ oligodendroglial cells in cortical layers V-VI (control, 665.1 ± 31.7 cells/mm^2; EAE 472.5 ± 18.3 cells/mm^2; $P = 0.0004$; Student's *t* test) that was associated with reduced numbers of mature oligodendrocytes and oligodendrocyte precursors (Supplementary Fig. 3f-g). These observations were partially mirrored in the hippocampal CA1 region (Supplementary Fig. 3j-l). Notably, there was a lower percentage of $CC1^+/Olig2^+$ mature oligodendrocytes and a higher percentage of $NG2^+$/Olig2 oligodendrocyte precursors in the demyelinating EAE cortex (Supplementary Fig. 3h) suggesting the activation of this cell population in an attempt to compensate for oligodendrocyte and myelin loss. Thus, astrocyte calcium signaling abnormalities encompass the loss of mature oligodendroglial cells likely underlying cortical demyelination during EAE.

Diminished neuronal activity and synapse loss preferentially affecting excitatory inputs are induced in rodent models of neuroinflammation that mimic cortical MS lesions (Jafari et al., 2021; Lagumersindez-Denis et al., 2017). Hence, we next sought to determine whether astrocyte dysfunction and cortical demyelination are associated with synaptic pathology at acute EAE disease. We did not find differences between naïve and EAE mice regarding cortical mRNA expression of neuron/synaptic markers such as synaptosome associated protein 25 (*Snap25*), syntaxin 1B (*Sytx1b*) and synapsin 1 (*Syn1*) (Supplementary Fig. 4a). Consistently, the density of excitatory synapses identified by immunostaining of the postsynaptic scaffold protein Homer-1 and the presynaptic synaptophysin remained largely unchanged in the EAE cortex (Supplementary Fig. 4b, c). Thus, cortical pathology during acute EAE disease does not appear to involve excitatory synapse loss. To further analyze the extent of synaptic pathology in the EAE mouse cortex we next evaluated the

features of cortical excitatory synaptic transmission using *ex vivo* electrophysiology. The synaptic input-output curves, the paired-pulse ratios, the synaptic fatigue and the AMPA/NMDA receptor relationship of EPSCs evoked in layer V cortical pyramidal neurons from mice during acute EAE did not differ from that in naïve animals suggesting intact excitatory transmission (Supplementary Fig. 5a-d). The frequency and the amplitude of miniature EPSCs (mEPSCs) was also undistinguishable between control and EAE mice further indicating unaltered excitatory synaptic input (Supplementary Fig. 5e). Of note, cortical neurons from EAE mice displayed mEPSCs of increased duration, augmented half-width and slower rise- and decay-phases (Supplementary Fig. 5f). These results are reminiscent of previous observations in the striatum and the cerebellum of EAE mice (Centonze et al., 2009; Mandolesi et al., 2013) and show that cortical astrocyte malfunction during autoimmune inflammation is associated with subtle changes in excitatory synaptic transmission.

Alterations of spontaneous glutamate transmission and synaptic plasticity during EAE mice have been linked to neuroinflammation mediated by infiltrating T lymphocytes, activated microglia and reactive astrocytes (Centonze et al., 2009; Habbas et al., 2015; Mandolesi et al., 2013). Thus, we next examined the somatosensory cortex for the presence of inflammatory responses during acute disease. Gene expression analysis evidenced elevated levels of chemokines and adhesion molecules involved in the recruitment of peripheral immune cells such C-C motif chemokine ligand 2 (*Ccl2*), C-X-C motif chemokine ligand 10 (*Cxcl10*) and intercellular adhesion molecule 1 (*Icam*) (Fig. 4a). We also observed a significant increase of the microglia/activation marker cluster of differentiation 68 (*Cd68*) as well as elevated expression levels of pro-inflammatory factors and molecules involved in EAE and MS pathogenesis such as tumor necrosis factor α (*Tnfa*), interleukin 1α (*Il1a*), and components of complement system. In particular, the expression levels of *C1q* and *C1qb* were upregulated by 2-fold whereas complement component 3 (*C3*) was increased by > 200-fold in the EAE cortex. We next performed immunohistochemistry experiments using infiltrating and tissue resident cell markers to investigate the origin of cortical inflammation during EAE. Immunofluorescence staining of CD3 revealed the presence of scattered T cells associated with the meninges that correlated with neurological severity at acute EAE disease (Spearman's $r = 0.8710$; $P = 0.0023$) (Fig. 4b) but the cortex was not infiltrated. These results suggest T cells are unlike to account for the cortical pathology associated with astrocyte dysfunction during EAE. We found elevated CD68 immunoreactivity and higher numbers of CD68-immunopositive pouches associated with cortical Iba-1 immunopositive profiles in cortical layers V-VI highlighting microglial activation in the somatosensory cortex of EAE mice during the acute phase of the disease (Fig. 4c, d). Lastly, we examined the EAE cortex for the presence of reactive astrocytes possibly associated with aberrant calcium signaling during EAE. Immunofluorescence staining of the astrocyte reactivity marker GFAP evidenced increased expression levels in deep cortical layers from mice at acute disease (Fig. 4e, f) that were corroborated by qPCR (Fig. 4a). Previous studies have established that induction of astrocytic C3 is associated with the acquisition of disease phenotypes that promote neuronal and oligodendrocyte demise in EAE mice and human MS (Hou et al., 2020; Liddelow et al., 2017; Moreno-García et al., 2020). Consistently, C3 immunoreactivity was increased in the cortical parenchyma of mice at acute EAE (Fig. 4g)

and colocalization analysis showed that GFAP immunopositive astrocytic processes display increased C3 expression during EAE (Fig. 4h). Taken together, these results demonstrate that cortical autoimmune demyelination involves the emergence of reactive astrocytes in an inflammatory milieu that exhibit pathogenic potential.

3.5. Neuroinflammatory mediators trigger aberrant astrocyte calcium signaling

We next asked whether astrocyte calcium signaling abnormalities in the cortex of EAE mice result from cell activation in an inflammatory milieu. To test this, we interrogated the calcium handling properties of astrocytes activated *in vitro* by incubation with the pro-inflammatory factors TNFα, IL-1α and C1q whose expression is associated to the emergence of neurotoxic reactive astrocytes (Guttenplan et al., 2021; Liddelow et al., 2017) and was significantly induced in the somatosensory cortex at acute disease (Fig. 4a). Astrocytes incubated with TNFα, IL-1α and C1q displayed upregulated expression of selected genes related to the phenotypic transformation of these cells during EAE and MS (Liddelow et al., 2017; Moreno-García et al., 2020) including complement component C3 (Supplementary Fig. 6). In parallel, we observed deregulated expression of a number of calcium signaling molecules including glutamate (*Grm1*, *Grm3*, *Grm5*) and ATP/adenosine receptors (*P2ry1*, *Adora1*), molecules related to endoplasmic reticulum calcium handling (*Itpr1*, *Ryr1*, *Ryr2*, *Ryr3*), and cytoplasmic calcium binding proteins (*S100b*) (Fig. 5a). Some of these changes paralleled observations in astrocytes purified during acute EAE (Fig. 3e). Particularly, *Grm3* and *S100b* showed decreased gene expression in both experimental settings. However, genes such as *Grm1* and *Grm5* showed opposite changes in cells activated *in vitro* and *in vivo*.

Next, we wondered whether the observed deficits in the expression calcium handling genes translated to deregulated cytosolic calcium dynamics in astrocytes activated *in vitro*. Calcium responses to the cannabinoid agonist WIN were below detection threshold in cultured astrocytes, probably reflecting low expression levels of the receptor protein in our *in vitro* experimental settings that were not modulated by inflammatory challenge (Fig. 5a). Conversely, ATP and glutamate receptor agonists elicited reliable cytosolic calcium signals in control conditions (Fig. 5b, c). Cells activated by pro-inflammatory factors showed aberrant responses to glutamate, LY354740 and ATP and while the effect of (S)DHPG on cytosolic calcium levels remained unaffected (Fig. 5c). Incubation with the blocker of the sarco/endoplasmic reticulum calcium ATPase (SERCA) pump thapsigargin increased cytosolic calcium to the same extent in control and activated astrocytes, ruling out significant alterations in the calcium content of this organelle (Fig. 5c). In order to corroborate these observations, we monitored astrocyte calcium responses using two-photon microscopy *ex vivo*. Cortical slices incubated with TNFα, IL-1α and C1q (30 min) showed increased calcium event probability of cortical astrocytes thus resembling astrocyte hyperactivity at acute EAE disease (Fig. 5d-f). However, the duration and amplitude of astrocytic calcium events in cortical slices incubated with the pro-inflammatory cocktail were similar to the control condition (Fig. 5f). We next examined receptor-mediated astrocyte calcium signals in slices incubate with TNFα, IL-1α and C1q. The calcium responses of cortical astrocytes to WIN, ATP and glutamate were significantly attenuated following short-term incubation with the pro-inflammatory cocktail (Fig. 5g-h). Thus, high

local levels of pro-inflammatory mediators trigger deficits in the calcium responses of cortical astrocytes that mimic alterations during EAE pathology. Overall, these observations suggest that inflammation-triggered astrocyte activation underlies dysfunctional calcium dynamics with potential implications in neuronal network function.

3.5.0.0.1. Cortical astrocyte-neuronal network interplay is disrupted during EAE—Altered tuning of neuronal activity by calcium-based astrocyte signaling has the potential to contribute to cortical dysfunction in MS (Shigetomi et al., 2016). Hence, in order to decipher the physiopathological outcome of aberrant astrocyte calcium signaling on the activity of cortical networks we performed electrophysiological recordings of layer V pyramidal neurons. As first approach to investigate gliotransmission in the EAE cortex, we monitored NMDA receptor-mediated slow inward currents (SICs) as electrophysiological readout for astrocytic glutamate release (Araque et al., 2014; Fellin et al., 2004; Perea and Araque, 2005). EAE did not alter the amplitude (control, 37.32 ± 3.21 pA; EAE, 40.18 ± 5.74 pA) and area (control, 3998 ± 693 pA*ms; EAE, 4216 ± 964 pA*ms) of SICs in cortical layer V pyramidal neurons. However, we found a significant increase in the frequency of SICs in EAE mice compared to naïve animals that resembles high levels of spontaneous astrocyte calcium activity measured *ex vivo* (Fig. 6a-c). Reports indicate that astrocyte calcium mobilization and subsequent gliotransmitter release by receptors coupled to $G_{i/o}$ and G_q proteins rely on the activation of IP_3R_2 receptors (Baraibar et al., 2023; Covelo and Araque, 2018; Di Castro et al., 2011; Durkee et al., 2019; Mariotti et al., 2016). Consistently, the frequency of SICs was significantly reduced in mice lacking IP_3R_2 (IP_3R_2-KO) both in control conditions and during EAE, thus corroborating the involvement of astrocyte calcium signaling in gliotransmitter release (Fig. 6b, c). Altogether, these results suggest that spontaneous calcium hyperactivity increases astrocytic glutamate release in the EAE cortex.

We next assessed cortical synaptic plasticity mechanisms that rely on astrocyte gliotransmitter release. We have recently shown that neuron-released endocannabinoids and astrocyte CB_1 receptors trigger short-term heteroneuronal synaptic depression mediated by ATP/adenosine as gliotransmitters in the somatosensory cortex (Baraibar et al., 2023). Thus, we next performed double patch-recordings of layer V pyramidal neurons and monitored excitatory postsynaptic currents (EPSCs) evoked by electrical stimulation of layer II-III in naïve and EAE mice sacrificed at acute disease (Fig. 7a). Consistent with our previous observations, depolarization of single layer V pyramidal neurons (ND) induced a transient depression of the synaptic transmission (Fig. 7b, *left panel*) in 14 out of 42 (33%) heteroneurons in non-immunized mice (Fig. 7c). We also observed a transient potentiation of the synaptic transmission (Fig. 7b, *right panel*) in 10 out of 42 (24%) heteroneurons (Fig. 7c). EAE induction did not modulate the size of heteroneuronal synaptic plasticity (depression or potentiation) (Fig. 7b). However, the number of cortical heteroneurons exhibiting synaptic depression after ND was drastically reduced during EAE (4 out of 49 cells; 8%) (Fig. 7c). Conversely, immunized mice showed a significant increase in the percentage of transiently potentiated heteroneuronal synapses following ND (21 out of 49 cells; 43%) (Fig. 7c). Consistent with CB_1 receptor mediated regulation, heteroneuronal synaptic depression and potentiation were abolished following bath perfusion of the

antagonist AM251 both in control and EAE mice (Fig. 7d). To further corroborate the role of astrocytic CB_1 receptors in heterosynaptic plasticity during EAE we selectively deleted the *Cnr1* gene by viral expression of Cre-recombinase under the control of the astroglial promoter GFAP in the somatosensory cortex of $CB_1^{f/f}$ mice (aCB_1-KO) (Baraibar et al., 2023). Heteroneuronal depression was fully abolished in aCB_1-KO mice in both in control and disease conditions (control, 0 out of 13 cells; EAE, 0 out 15 cells) (Fig. 7c). Finally, heteroneuronal potentiation was also markedly reduced in naive and EAE aCB_1-KO mice (control, 1 out of 13 cells; EAE, 1 out of 15 cells) (Fig. 7c). These observations suggest that EAE shifts short-term plasticity mediated by astrocyte CB_1 receptors towards synaptic potentiation.

To further corroborate the hypothesis that autoimmune inflammation impairs astrocyte-mediated modulation of cortical synaptic function we next investigated long-term plasticity mechanisms that depend on astrocytic calcium signaling during EAE. Endocannabinoids and astrocyte CB_1 receptors gate a form of spike timing-dependent long-term plasticity (STDP) in the neonatal mouse that relies on the astrocytic delivery of glutamate as gliotransmitter and switches to long-term potentiation at more mature stages (Martínez-Gallego et al., 2022; Min and Nevian, 2012). Thus, we next investigated the possible alterations in STDP in the EAE cortex. With this aim, we recorded EPSCs at layer II-III to layer V synapses onto pyramidal neurons and induced STDP by pairing each EPSC with a preceding postsynaptically evoked action potential (AP-EPSP pairing, timing interval $\Delta t = -25$ ms, 60 AP-EPSP pairings in 10 min). This stimulation protocol induced mild long-term potentiation of synaptic transmission in good agreement with previous observations in the adult mouse neocortex (Fig. 7e-f) (Martínez-Gallego et al., 2022). Remarkably, the STDP induction protocol resulted in a significantly augmented potentiation of cortical synaptic transmission in EAE mice (Fig. 7e-f). We next aimed at corroborating the role of astrocyte CB_1 receptors as mediators of STDP in control and disease conditions. Bath application of AM251 prevented the expression of STDP both in naïve mice and during EAE, suggesting that both phenomena were mediated by CB_1 receptors (Fig. 7f). STDP was also abolished in control and immunized aCB_1-KO mice further suggesting that astrocyte CB_1 receptors trigger the potentiation of excitatory transmission in control and disease conditions (Fig. 7f). The STDP induction protocol elicited a slight potentiation of synaptic transmission in control $CB_1^{f/f}$ mice injected with AAV9-GFAP-mCherry (aCB_1) that was significantly augmented during acute EAE thus corroborating the results obtained in non-transgenic mice (Fig. 7f). Finally, we examined the dependency of STDP on astrocytic calcium using IP_3R_2-KO mice in which G protein-mediated calcium signal is selectively impaired in astrocytes (Baraibar et al., 2023; Di Castro et al., 2011). Consistent with our observations in aCB_1-KO mice, both the spike-timing dependent potentiation recorded in control conditions and at acute EAE disease were absent in IP_3R_2-KO mice (Fig. 7f). Altogether, these results show that EAE disrupts cortical synaptic plasticity mechanisms triggered by astrocyte CB_1 receptors, eventually causing neuronal network hyperactivity.

4. Discussion

Cortical dysfunction is a core pathological feature of MS that underlies cognitive deficits and predicts disease progression (Calabrese et al., 2015; Mahad et al., 2015). Neuronal

and synaptic failure have been studied extensively in patients and animal models of the disease and are postulated at the origin of functional deficits in cortical MS (Jafari et al., 2021; Jürgens et al., 2016). Astrocytes fine-tune neuronal network operation through the release of gliotransmitters (Araque et al., 2014) and have been crucially involved in MS pathophysiology (Linnerbauer et al., 2020). However, the contribution of astroglial cells to MS cortical network dysfunction has remained largely unknown. In this study we investigated the calcium activity of cortical astrocytes and the features of gliotransmission in a mouse model of MS. Applying two-photon imaging *ex vivo* we discovered the emergence of dysfunctional astrocyte activity patterns during EAE progression consisting in calcium events of increased frequency and duration. This results highlight hyperactive states of astrocytes during autoimmune demyelination with potential physiopathological outcomes on cortical information processing that would benefit from *in vivo* analysis. The calcium signal is an intricate phenomenon and, at the present time, the physiological meaning of the complex spatial and temporal properties of astrocyte calcium responses remain elusive in spite of the great effort that has been and still is being made (for review see Rusakov, 2015; Volterra et al., 2014; Yu et al., 2020). Further studies, out of the scope of the present work, are thus needed to understand the repercussions of the altered calcium signal properties observed in EAE animals in terms of cortical dysfunction. From a mechanistic perspective, our results show that astrocyte calcium hyperexcitability in the somatosensory cortex is mostly independent on neuronal activity and suggests that autoimmune demyelination alters the intrinsic activity of cortical astrocytes, in line with recent observations in mouse models of α-synucleinopathies (Nanclares et al., 2023). These observations are in line with recent reports of astrocyte hyperactivity in mouse models of AD using *in vivo* multiphoton microscopy (Delekate et al., 2014; Lines et al., 2022), although decreased calcium signaling has also been reported at early stages of Alheimer's disease pathology (Shah et al., 2022). These apparent discrepancies might be explained on the basis that reactive astrocyte responses differ across specific anatomical regions, neuroinflammatory states and severity of the neurodegenerative process (Hasel et al., 2021; Patani et al., 2023; Sofroniew, 2020). Although further efforts are required to delineate the features and mechanistic basis of astrocyte network dysfunction in CNS disorders, in the context of previous studies our results suggest that astrocyte calcium deregulation is a consistent finding in neuroinflammatory and neurodegenerative conditions beyond amyloid-β and α-synuclein pathology, with potential implications for disease symptomatology and progression.

Deregulated astrocyte calcium excitability in the EAE cortex was encompassed by diminished responses mediated by astroglial CB_1 receptors both *ex vivo* and *in vivo*. This functional deficit might reflect reductions in the astrocyte-associated CB_1 receptor pools during acute disease (Moreno-García et al., 2020) and/or be associated with the deregulation of intracellular calcium signaling machinery as suggested by our targeted gene expression analysis. Notably, the astrocyte hypo-responsiveness to CB_1 receptor activation was mirrored by deficits in the calcium activity of astrocytes to ATP, glutamate and selective $mGluR_{1/5}$ and $mGluR_{2/3}$ agonists, further suggesting a widespread deregulation of astrocyte calcium signaling pathways during autoimmune inflammation. These observations are reminiscent of recent reports of spontaneous hyperactivity but

reduced sensory-evoked astrocyte responsiveness in experimental Alzheimer's disease (Lines et al., 2022). Irrespective of the precise mechanisms underlying astrocyte calcium hypo-responsiveness to acute activation, the emerging picture is that impaired activity mediated by endocannabinoids, ATP/adenosine or glutamate as neurotransmitters may contribute to dysfunctional astrocytic calcium dynamics in the MS cortex.

Activation of astrocytes by either G_i- or G_q-DREADDs increased the frequency and amplitude of calcium signals as consistent with previous studies using pharmacogenetic tools (Baraibar et al., 2023; Durkee et al., 2019), as well as pharmacological or sensory-evoked astrocyte stimulation (Ding et al., 2013; Jiang et al., 2016; Lines et al., 2020; Wang et al., 2006). Mechanistically, we show that deficits in astrocyte calcium responses to neurotransmitter receptors in the EAE cortex rely on impaired activity of both G_i and G_q protein signaling pathways, as concluded from the impaired responses to pharmacological activation of DREADDs expressing cells. An interesting observation from our pharmacogenetic experiments is that calcium signaling mediated by astrocyte G_i proteins is predominantly altered in cortical astrocytes during autoimmune inflammation as compared to G_q protein-dependent calcium mechanisms. These observations confirm the importance of the G_i protein signaling pathway in astrocyte physiology (Covelo and Araque, 2018; Jiang et al., 2016; Mariotti et al., 2016) and highlight its relevance for the acquisition of astrocyte disease phenotypes linked to MS.

In this study we establish a mechanistic association between cortical autoimmune neuroinflammation and the emergence of aberrant astrocyte phenotypes at the calcium excitability level. The presence of reactive astrocytes expressing complement C3 was linked to elevated levels pro-inflammatory factors in the EAE cortex including the microglia-secreted cytokines TNFα, IL-1α and C1q (Clarke et al., 2018; Liddelow et al., 2017). Remarkably, acute slice activation with a pro-inflammatory cocktail composed of TNFα, IL-1α and C1q reproduced spontaneous astrocyte hyperactivity at the calcium event frequency level and hypo-responsiveness to ATP and glutamate, thus mirroring observations in the EAE cortex. However, incubation with pro-inflammatory factors did not mirror the increased duration and amplitude of astrocyte calcium events in cortical slices from EAE mice. On mechanistic grounds, using an *in vitro* setting we demonstrate cell-autonomous effects of pro-inflammatory astrocyte activation with TNFα, IL-1α and C1q on the expression of calcium handling molecules, encompassed by dysfunctional calcium responses to receptor agonists. Despite discrepancies regarding deregulation of spontaneous astrocyte calcium fluctuations between EAE and acute inflammatory models, these results highlight the relevance of TNFα, IL-1α and C1q as major upstream mediators of dysfunctional astrocyte calcium signaling in the MS cortex. Future assessments in EAE mice undergoing antiinflammatory treatments and/or in triple knockout mice lacking expression of these cytokines (Clarke et al., 2018; Hartmann et al., 2019) may help elucidate the relevance of pro-inflammatory signals in the emergence of aberrant astrocyte signaling and their potential for astrocyte therapeutic targeting in cortical MS.

Our observations in cultured cells are in good agreement with previously published results showing that inflammatory astrocyte activation with TGF-ß1, LPS and IFNγ significantly deregulates, mostly down, astrocyte calcium signaling both at the gene expression and

functional levels, in parallel to the upregulation of immune signaling and cell injury molecular networks (Hamby et al., 2012). Our gene expression results in cultured cells highlight commonly down-regulated genes, such as *P2ry1* and *Adora1*, but also certain discrepancies most likely related to the different pro-inflammatory stimuli used. In the same line, we observed several inconsistencies regarding deregulation of calcium handling molecules between EAE astrocytes and cultured cells activated with TNFα, IL-1α and C1q which may reflect a more complex and dynamic deregulation of calcium signaling in astroglia dynamically activated in the evolving inflammatory context of ongoing autoimmune demyelination. Indeed, gene expression analysis of astrocytes purified at acute EAE disease or cultured cells following 24 h exposure to selected pro-inflammatory factors are two fundamentally different manipulations that may well lead to some inconsistencies associated to the fact that *in vitro* model is far from mirroring the complex and evolving neuroinflammatory context of ongoing autoimmune demyelination. In support of this hypothesis, astrocytes inflammatory transitions during acute systemic inflammation induced by LPS change dramatically over time and cluster in a layer-specific manner within the mouse cortex (Hasel et al., 2021). Altogether, these results support the emerging concept that reactive astrogliosis is associated with neuroinflammatory context-specific deficits in calcium signaling mechanisms that feature heterogeneous populations of dysfunctional astrocytes contributing to neuro-pathologies (Hasel et al., 2021; Patani et al., 2023; Sofroniew, 2020). On the other hand, results in cultured astrocytes reproduce certain features of astrocyte calcium dysfunction in the EAE cortex such as the reduced *Gmr3* expression and attenuated calcium responses to agonist activation of mGluR2/3. These combined observations suggest that deregulation of astrocyte calcium handling properties during autoimmune demyelination results in part from direct inflammation-mediated signaling onto astroglial cells, which may be further addressed at a mechanistic level in future studies using culture systems.

A remarkable finding in this study is that altered astrocyte calcium excitability encompasses aberrant cortical gliotransmission during autoimmune inflammation. We show that the frequency of SICs is increased in the EAE cortex highlighting an exacerbated release of glutamate from reactive astrocytes that mirrors recent observations in rodent models of Alzheimer's disease (Lines et al., 2022; Talantova et al., 2013). Furthermore, our results unveil that short-term and long-term plasticity mechanisms mediated by astrocyte CB_1 receptors in the brain cortex (Baraibar et al., 2023; Martínez-Gallego et al., 2022; Min and Nevian, 2012) shift to potentiation during autoimmune demyelination. Thus, deficits in astrocyte CB_1 receptor mediated calcium signaling translate into gliotransmission defects leading to the potentiation of cortical excitation. Strikingly, our electrophysiological results suggest that heterosynaptic and spike-timing dependent plasticity mechanisms in the inflamed cortex still depend on intracellular calcium mobilization following the activation of the astrocytic CB_1 receptor pool. Altogether, our results suggest that functional reshaping of astrocyte-neuron networks during autoimmune demyelination involves complex adaptations in calcium signal-to-noise ratio that lead to deregulation in the identity and/or relative amount of gliotransmitters shaping cortical synaptic excitation.

Concerning the pathogenic implications of dysfunctional astrocyte calcium signaling in cortical MS, emerging evidence shows that deregulation in the calcium dynamics of

astroglial cells affect neuronal network function leading to behavioral abnormalities in neurodegenerative diseases (Nagai et al., 2021; Shah et al., 2022; Shigetomi et al., 2016). In this context, the results of the present study suggest that dysfunction of astrocyte-neuronal interplay may deregulate cortical electrical activity and contribute to cognitive decline in MS patients. Also related to the pathogenesis of cognitive and memory impairments, it is well established that MS cortical pathology involves early excitatory-inhibitory imbalance leading and synaptic loss and neurodegeneration (Calabrese et al., 2015; Ellwardt et al., 2018; Jafari et al., 2021; Jürgens et al., 2016; Potter et al., 2016). Of note, exacerbated release of glutamate from astrocytes is postulated to contribute to neuronal excitotoxicity and synapse loss in status epilepticus and Alzheimer's disease, supporting the neurotoxic potential of aberrant gliotransmission in neurodegenerative and neuroinflammatory conditions (Ding et al., 2007; Talantova et al., 2013). In this study, dysfunctional astrocyte calcium activity and gliotransmission were not associated with significant synaptic deficits or synapse loss in the EAE cortex at acute disease. However, our electrophysiological analysis shows increased duration of mEPSCs in layer V pyramidal neurons reminiscent of previous observations in the striatum and cerebellum of EAE mice (Centonze et al., 2009; Mandolesi et al., 2013). These observations suggest that aberrant gliotransmission encompasses early cortical excitatory synaptic imbalance and supports the possibility that astrocyte dysfunction leading to exacerbated excitatory transmission contributes to synaptic deregulation and neurodegeneration in MS.

In summary, the present study provides key findings on the role of astrocytes in cortical MS pathology. We have shown that cortical astrocytes activated in an inflammatory milieu are spontaneously hyperactive but hypo-responsive to receptor-mediated calcium signaling. Aberrant calcium excitability encompasses astrocyte-to-neuron communication defects leading to the potentiation of excitatory transmission. These observations suggest that deregulated astrocyte calcium signaling and gliotransmission contribute to abnormal cortical network operation in MS thus pointing to novel therapeutic targets against cognitive decline.

Supplementary Material

Refer to Web version on PubMed Central for supplementary material.

Acknowledgements

We would like to thank the personnel of the Animal Facilities of the University of the Basque Country and Neurocentre Magendie for mouse care. We also thank G. Perea for providing inositol 1,4,5-trisphosphate receptor type 2 knockout (IP_3R_2-KO) mice, and S. Calovi and F.N. Soria for support in the analysis of confocal images.

Funding

This work was funded by the Instituto de Salud Carlos III (PI21/00629, to S.M. and A.R.-A; CB06/05/00, to C.M.) and cofounded by the European Union, Basque Government (PIBA_2023_1_0046; 2023111031; IT1473-22, to S.M.; IT1203-19, to C.M.), ARSEP Foundation (ARSEP - 1310 to S.M. and G.M.), INSERM (to G.M.), the European Research Council (MiCaBra, ERC-2017-AdG-786467, to G.M.), Fondation pour la Recherche Medicale (FRM, DRM20101220445 to G.M.), Region Aquitaine (CanBrain, AAP2022A-2021-16763610 and -17219710 to G.M.); French State/Agence Nationale de la Recherche (HippObese, ANR-23-ce14-0004-03; ERA-Net Neuron CanShank, ANR-21-NEU2-0001-04, to G.M), La Caixa Research Health 2023 (Psycho-Cannabis, HR23-00793, to G.M.), Spanish Ministry of Science and Innovation (PID2019-109724RB-100 to C.M.; PGC2018-093990-A-I00, to E.S.-G.), National Institutes of Health-MH (MH, R01MH119355; NINDS, R01NS097312; NIDA, R01DA048822,

to A.A.), Postdoctoral and Predoctoral Programs of the Basque Government (to A.M.B., T.C. A.M.-G., and C.U), Predoctoral Program of the UPV/EHU (to E.S.).

Data availability

All data are available in the main text and the Supplementary materials or from the corresponding author on reasonable request.

References

Akerboom J, Carreras Calderón N, Tian L, Wabnig S, Prigge M, Tolö J, Gordus A, Orger MB, Severi KE, Macklin JJ, Patel R, Pulver SR, Wardill TJ, Fischer E, Schüler C, Chen TW, Sarkisyan KS, Marvin JS, Bargmann CI, Kim DS, Kügler S, Lagnado L, Hegemann P, Gottschalk A, Schreiter ER, Looger LL, 2013. Genetically encoded calcium indicators for multi-color neural activity imaging and combination with optogenetics. Front. Mol. Neurosci 6, 2. 10.3389/fnmol.2013.00002. [PubMed: 23459413]

Araque A, Carmignoto G, Haydon PG, Oliet SH, Robitaille R, Volterra A, 2014. Gliotransmitters travel in time and space. Neuron 81 (4), 728–739. 10.1016/j.neuron.2014.02.007. [PubMed: 24559669]

Baker D, Pryce G, Croxford JL, Brown P, Pertwee RG, Makriyannis A, Khanolkar A, Layward L, Fezza F, Bisogno T, Di Marzo V, 2001. Endocannabinoids control spasticity in a multiple sclerosis model. FASEB J. 15 (2), 300–302. 10.1096/fj.00-0399fje. [PubMed: 11156943]

Baraibar AM, Belisle L, Marsicano G, Matute C, Mato S, Araque A, Kofuji P, 2023. Spatial organization of neuron-astrocyte interactions in the somatosensory cortex. Cereb. Cortex 33 (8), 4498–4511. 10.1093/cercor/bhac357. [PubMed: 36124663]

Calabrese M, Rocca MA, Atzori M, Mattisi I, Favaretto A, Perini P, Gallo P, Filippi M, 2010. A 3-year magnetic resonance imaging study of cortical lesions in relapse-onset multiple sclerosis. Ann. Neurol 67 (3), 376–383. 10.1002/ana.21906. [PubMed: 20373349]

Calabrese M, Magliozzi R, Ciccarelli O, Geurts JJ, Reynolds R, Martin R, 2015. Exploring the origins of grey matter damage in multiple sclerosis. Nat. Rev. Neurosci 16 (3), 147–158. 10.1038/nrn3900. [PubMed: 25697158]

Centonze D, Bari M, Rossi S, Prosperetti C, Furlan R, Fezza F, De Chiara V, Battistini L, Bernardi G, Bernardini S, Martino G, Maccarrone M, 2007. The endocannabinoid system is dysregulated in multiple sclerosis and in experimental autoimmune encephalomyelitis. Brain 130 (Pt 10), 2543–2553. 10.1093/brain/awm160. [PubMed: 17626034]

Centonze D, Muzio L, Rossi S, Cavasinni F, De Chiara V, Bergami A, Musella A, D'Amelio M, Cavallucci V, Martorana A, Bergamaschi A, Cencioni MT, Diamantini A, Butti E, Comi G, Bernardi G, Cecconi F, Battistini L, Furlan R, Martino G, 2009. Inflammation triggers synaptic alteration and degeneration in experimental autoimmune encephalomyelitis. J. Neurosci 29 (11), 3442–3452. 10.1523/JNEUROSCI.5804-08.2009. [PubMed: 19295150]

Chao CC, Gutiérrez-Vázquez C, Rothhammer V, Mayo L, Wheeler MA, Tjon EC, Zandee SEJ, Blain M, de Lima KA, Takenaka MC, Avila-Pacheco J, Hewson P, Liu L, Sanmarco LM, Borucki DM, Lipof GZ, Trauger SA, Clish CB, Antel JP, Prat A, Quintana FJ, 2019. Metabolic control of astrocyte pathogenic activity via cPLA2-MAVS. Cell 179 (7), 1483–1498.e1422. 10.1016/j.cell.2019.11.016. [PubMed: 31813625]

Clarke LE, Liddelow SA, Chakraborty C, Münch AE, Heiman M, Barres BA, 2018. Normal aging induces A1-like astrocyte reactivity. PNAS 115 (8), E1896–E1905. 10.1073/pnas.1800165115. [PubMed: 29437957]

Covelo A, Araque A, 2018. Neuronal activity determines distinct gliotransmitter release from a single astrocyte. Elife 7. 10.7554/eLife.32237.

De Stefano N, Matthews PM, Filippi M, Agosta F, De Luca M, Bartolozzi ML, Guidi L, Ghezzi A, Montanari E, Cifelli A, Federico A, Smith SM, 2003. Evidence of early cortical atrophy in MS: relevance to white matter changes and disability. Neurology 60 (7), 1157–1162. 10.1212/01.wnl.0000055926.69643.03. [PubMed: 12682324]

Delekate A, Füchtemeier M, Schumacher T, Ulbrich C, Foddis M, Petzold GC, 2014. Metabotropic P2Y1 receptor signalling mediates astrocytic hyperactivity in vivo in an Alzheimer's disease mouse model. Nat. Commun 5, 5422. 10.1038/ncomms6422. [PubMed: 25406732]

Di Castro MA, Chuquet J, Liaudet N, Bhaukaurally K, Santello M, Bouvier D, Tiret P, Volterra A, 2011. Local Ca^{2+} detection and modulation of synaptic release by astrocytes. Nat. Neurosci 14 (10), 1276–1284. 10.1038/nn.2929. [PubMed: 21909085]

Ding S, Fellin T, Zhu Y, Lee SY, Auberson YP, Meaney DF, Coulter DA, Carmignoto G, Haydon PG, 2007. Enhanced astrocytic Ca2+ signals contribute to neuronal excitotoxicity after status epilepticus. J. Neurosci 27, 10674–10684. 10.1523/JNEUROSCI.2001-07.2007. [PubMed: 17913901]

Ding F, O'Donnell J, Thrane AS, Zeppenfeld D, Kang H, Xie L, Wang F, Nedergaard M, 2013. α1-Adrenergic receptors mediate coordinated Ca^{2+} signaling of cortical astrocytes in awake, behaving mice. Cell Calcium 54 (6), 387–394. 10.1016/j.ceca.2013.09.001. [PubMed: 24138901]

Durkee CA, Covelo A, Lines J, Kofuji P, Aguilar J, Araque A, 2019. $G_{i/o}$ protein-coupled receptors inhibit neurons but activate astrocytes and stimulate gliotransmission. Glia 67 (6), 1076–1093. 10.1002/glia.23589. [PubMed: 30801845]

Eljaschewitsch E, Witting A, Mawrin C, Lee T, Schmidt PM, Wolf S, Hoertnagl H, Raine CS, Schneider-Stock R, Nitsch R, Ullrich O, 2006. The endocannabinoid anandamide protects neurons during CNS inflammation by induction of MKP-1 in in microglial cells. Neuron 49 (1), 67–79. 10.1016/j.neuron.2005.11.027. [PubMed: 16387640]

Ellwardt E, Pramanik G, Luchtman D, Novkovic T, Jubal ER, Vogt J, Arnoux I, Vogelaar CF, Mandal S, Schmalz M, Barger Z, Ruiz de Azua I, Kuhlmann T, Lutz B, Mittmann T, Bittner S, Zipp F, Stroh A, 2018. Maladaptive cortical hyperactivity upon recovery from experimental autoimmune encephalomyelitis. Nat. Neurosci 21 (10), 1392–1403. 10.1038/s41593-018-0193-2. [PubMed: 30258239]

Errede M, Girolamo F, Ferrara G, Strippoli M, Morando S, Boldrin V, Rizzi M, Uccelli A, Perris R, Bendotti C, Salmona M, Roncali L, Virgintino D, 2012. Blood-brain barrier alterations in the cerebral cortex in experimental autoimmune encephalomyelitis. J. Neuropathol. Exp. Neurol 71, 840–854. 10.1097/NEN.0b013e31826ac110. [PubMed: 23001217]

Eshaghi A, Prados F, Brownlee WJ, Altmann DR, Tur C, Cardoso MJ, De Angelis F, van de Pavert SH, Cawley N, De Stefano N, Stromillo ML, Battaglini M, Ruggieri S, Gasperini C, Filippi M, Rocca MA, Rovira A, Sastre-Garriga J, Vrenken H, Leurs CE, Killestein J, Pirpamer L, Enzinger C, Ourselin S, Wheeler-Kingshott CAMG, Chard D, Thompson AJ, Alexander DC, Barkhof F, Ciccarelli O, 2018. Deep gray matter volume loss drives disability worsening in multiple sclerosis. Ann. Neurol 83 (2), 210–222. 10.1002/ana.25145. [PubMed: 29331092]

Feinstein A, Magalhaes S, Richard JF, Audet B, Moore C, 2014. The link between multiple sclerosis and depression. Nat. Rev. Neurol 10 (9), 507–517. 10.1038/nrneurol.2014.139. [PubMed: 25112509]

Fellin T, Pascual O, Gobbo S, Pozzan T, Haydon PG, Carmignoto G, 2004. Neuronal synchrony mediated by astrocytic glutamate through activation of extrasynaptic NMDA receptors. Neuron 43 (5), 729–743. 10.1016/j.neuron.2004.08.011. [PubMed: 15339653]

Girolamo F, Ferrara G, Strippoli M, Rizzi M, Errede M, Trojano M, Perris R, Roncali L, Svelto M, Mennini T, Virgintino D, 2011. Cerebral cortex demyelination and oligodendrocyte precursor response to experimental autoimmune encephalomyelitis. Neurobiol. Dis 43, 678–689. 10.1016/j.nbd.2011.05.021. [PubMed: 21679768]

Guttenplan KA, Weigel MK, Prakash P, Wijewardhane PR, Hasel P, Rufen-Blanchette U, Münch AE, Blum JA, Fine J, Neal MC, Bruce KD, Gitler AD, Chopra G, Liddelow SA, Barres BA, 2021. Neurotoxic reactive astrocytes induce cell death via saturated lipids. Nature 599 (7883), 102–107. 10.1038/S41586-021-03960-y. [PubMed: 34616039]

Habbas S, Santello M, Becker D, Stubbe H, Zappia G, Liaudet N, Klaus FR, Kollias G, Fontana A, Pryce CR, Suter T, Volterra A, 2015. Neuroinflammatory TNFα Impairs Memory via Astrocyte Signaling. Cell 163 (7), 1730–1741. 10.1016/j.cell.2015.11.023. [PubMed: 26686654]

Hamby ME, Coppola G, Ao Y, Geschwind DH, Khakh BS, Sofroniew MV, 2012. Inflammatory mediators alter the astrocyte transcriptome and calcium signaling elicited by multiple G-protein-

coupled receptors. J. Neurosci 32 (42), 14489–14510. 10.1523/JNEUROSCI.1256-12.2012. [PubMed: 23077035]

Han J, Kesner P, Metna-Laurent M, Duan T, Xu L, Georges F, Koehl M, Abrous DN, Mendizabal-Zubiaga J, Grandes P, Liu Q, Bai G, Wang W, Xiong L, Ren W, Marsicano G, Zhang X, 2012. Acute cannabinoids impair working memory through astroglial CB_1 receptor modulation of hippocampal LTD. Cell 148 (5), 1039–1050. 10.1016/j.cell.2012.01.037. [PubMed: 22385967]

Hartmann K, Sepulveda-Falla D, Rose IVL, Madore C, Muth C, Matschke J, Butovsky O, Liddelow S, Glatzel M, Krasemann S, 2019. Complement 3+- astrocytes are highly abundant in prion diseases, but their abolishment led to an accelerated disease course and early dysregulation of microglia. Acta Neuropathol. Commun 7 (1), 83. 10.1186/s40478-019-0735-1. [PubMed: 31118110]

Hasel P, Rose IVL, Sadick JS, Kim RD, Liddelow SA, 2021. Neuroinflammatory astrocyte subtypes in the mouse brain. Nat. Neurosci 24 (10), 1475–1487. 10.1038/s41593-021-00905-6. [PubMed: 34413515]

Haustein MD, Kracun S, Lu XH, Shih T, Jackson-Weaver O, Tong X, Xu J, Yang XW, O'Dell TJ, Marvin JS, Ellisman MH, Bushong EA, Looger LL, Khakh BS, 2014. Conditions and constraints for astrocyte calcium signaling in the hippocampal mossy fiber pathway. Neuron 82 (2), 413–429. 10.1016/j.neuron.2014.02.041. [PubMed: 24742463]

Hirrlinger PG, Scheller A, Braun C, Hirrlinger J, Kirchhoff F, 2006. Temporal control of gene recombination in astrocytes by transgenic expression of the tamoxifen-inducible DNA recombinase variant CreERT2. Glia 54 (1), 11–20. 10.1002/glia.20342. [PubMed: 16575885]

Hou B, Zhang Y, Liang P, He Y, Peng B, Liu W, Han S, Yin J, He X, 2020. Inhibition of the NLRP3-inflammasome prevents cognitive deficits in experimental autoimmune encephalomyelitis mice via the alteration of astrocyte phenotype. Cell Death Dis. 11 (5), 377. 10.1038/s41419-020-2565-2. [PubMed: 32415059]

Jafari M, Schumacher AM, Snaidero N, Ullrich Gavilanes EM, Neziraj T, Kocsis-Jutka V, Engels D, Jürgens T, Wagner I, Weidinger JDF, Schmidt SS, Beltrán E, Hagan N, Woodworth L, Ofengeim D, Gans J, Wolf F, Kreutzfeldt M, Portugues R, Merkler D, Misgeld T, Kerschensteiner M, 2021. Phagocyte-mediated synapse removal in cortical neuroinflammation is promoted by local calcium accumulation. Nat. Neurosci 24 (3), 355–367. 10.1038/S41593-020-00780-7. [PubMed: 33495636]

Jiang R, Diaz-Castro B, Looger LL, Khakh BS, 2016. Dysfunctional Calcium and Glutamate signaling in striatal astrocytes from Huntington's disease model mice. J. Neurosci 36 (12), 3453–3470. 10.1523/JNEUROSCI.3693-15.2016. [PubMed: 27013675]

Jürgens T, Jafari M, Kreutzfeldt M, Bahn E, Brück W, Kerschensteiner M, Merkler D, 2016. Reconstruction of single cortical projection neurons reveals primary spine loss in multiple sclerosis. Brain 139 (Pt 1), 39–46. 10.1093/brain/awv353. [PubMed: 26667278]

Lagumersindez-Denis N, Wrzos C, Mack M, Winkler A, van der Meer F, Reinert MC, Hollasch H, Flach A, Brühl H, Cullen E, Schlumbohm C, Fuchs E, Linington C, Barrantes-Freer A, Metz I, Wegner C, Liebetanz D, Prinz M, Brück W, Stadelmann C, Nessler S, 2017. Differential contribution of immune effector mechanisms to cortical demyelination in multiple sclerosis. Acta Neuropathol. 134 (1), 15–34. 10.1007/s00401-017-1706-x. [PubMed: 28386765]

Liddelow SA, Guttenplan KA, Clarke LE, Bennett FC, Bohlen CJ, Schirmer L, Bennett ML, Münch AE, Chung WS, Peterson TC, Wilton DK, Frouin A, Napier BA, Panicker N, Kumar M, Buckwalter MS, Rowitch DH, Dawson VL, Dawson TM, Stevens B, Barres BA, 2017. Neurotoxic reactive astrocytes are induced by activated microglia. Nature 541 (7638), 481–487. 10.1038/nature21029. [PubMed: 28099414]

Lines J, Martin ED, Kofuji P, Aguilar J, Araque A, 2020. Astrocytes modulate sensory-evoked neuronal network activity. Nat. Commun 11 (1), 3689. 10.1038/s41467-020-17536-3. [PubMed: 32704144]

Lines J, Baraibar AM, Fang C, Martin ED, Aguilar J, Lee MK, Araque A, Kofuji P, 2022. Astrocyte-neuronal network interplay is disrupted in Alzheimer's disease mice. Glia 70 (2), 368–378. 10.1002/glia.24112. [PubMed: 34726298]

Linnerbauer M, Wheeler MA, Quintana FJ, 2020. Astrocyte crosstalk in CNS inflammation. Neuron 108 (4), 608–622. 10.1016/j.neuron.2020.08.012. [PubMed: 32898475]

Lütcke H, Murayama M, Hahn T, Margolis DJ, Astori S, Zum Alten Borgloh SM, Göbel W, Yang Y, Tang W, Kügler S, Sprengel R, Nagai T, Miyawaki A, Larkum ME, Helmchen F, Hasan MT, 2010. Optical recording of neuronal activity with a genetically-encoded calcium indicator in anesthetized and freely moving mice. Front. Neural Circuits 4, 9. 10.3389/fncir.2010.00009. [PubMed: 20461230]

Mahad DH, Trapp BD, Lassmann H, 2015. Pathological mechanisms in progressive multiple sclerosis. Lancet Neurol. 14 (2), 183–193. 10.1016/S1474-4422(14)70256-X. [PubMed: 25772897]

Mandolesi G, Musella A, Gentile A, Grasselli G, Haji N, Sepman H, Fresegna D, Bullitta S, De Vito F, Musumeci G, Di Sanza C, Strata P, Centonze D, 2013. Interleukin-1β alters glutamate transmission at purkinje cell synapses in a mouse model of multiple sclerosis. J. Neurosci 33 (29), 12105–12121. 10.1523/JNEUROSCI.5369-12.2013. [PubMed: 23864696]

Mariotti L, Losi G, Sessolo M, Marcon I, Carmignoto G, 2016. The inhibitory neurotransmitter GABA evokes long-lasting Ca(2+) oscillations in cortical astrocytes. Glia 64 (3), 363–373. 10.1002/glia.22933. [PubMed: 26496414]

Marsicano G, Wotjak CT, Azad SC, Bisogno T, Rammes G, Cascio MG, Hermann H, Tang J, Hofmann C, Zieglgänsberger W, Di Marzo V, Lutz B, 2002. The endogenous cannabinoid system controls extinction of aversive memories. Nature 418 (6897), 530–534. 10.1038/nature00839. [PubMed: 12152079]

Martínez-Gallego I, Pérez-Rodríguez M, Coatl-Cuaya H, Flores G, Rodríguez-Moreno A, 2022. Adenosine and astrocytes determine the developmental dynamics of spike timing-dependent plasticity in the somatosensory cortex. J. Neurosci 42 (31), 6038–6052. 10.1523/JNEUROSCI.0115-22.2022. [PubMed: 35768208]

Min R, Nevian T, 2012. Astrocyte signaling controls spike timing-dependent depression at neocortical synapses. Nat. Neurosci 15 (5), 746–753. 10.1038/nn.3075. [PubMed: 22446881]

Moreno-García Á, Bernal-Chico A, Colomer T, Rodríguez-Antigüedad A, Matute C, Mato S, 2020. Gene expression analysis of astrocyte and microglia Endocannabinoid signaling during autoimmune demyelination. Biomolecules 10 (9). 10.3390/biom10091228.

Nagai J, Bellafard A, Qu Z, Yu X, Ollivier M, Gangwani MR, Diaz-Castro B, Coppola G, Schumacher SM, Golshani P, Gradinaru V, Khakh BS, 2021. Specific and behaviorally consequential astrocyte Gq GPCR signaling attenuation *in vivo* with iβARK. Neuron 109 (14), 2256–2267. 10.1016/j.neuron.2021.05.023. [PubMed: 34139149]

Nanclares C, Poynter J, Martell-Martinez HA, Vermilyea S, Araque A, Kofuji P, Lee MK, Covelo A, 2023. Dysregulation of astrocytic Ca^{2+} signaling and gliotransmitter release in mouse models of α-synucleinopathies. Acta Neuropathol. 145 (5), 597–610. 10.1007/s00401-023-02547-3. [PubMed: 36764943]

Navarrete M, Araque A, 2010. Endocannabinoids potentiate synaptic transmission through stimulation of astrocytes. Neuron 68 (1), 113–126. 10.1016/j.neuron.2010.08.043. [PubMed: 20920795]

Ohkura M, Sasaki T, Sadakari J, Gengyo-Ando K, Kagawa-Nagamura Y, Kobayashi C, Ikegaya Y, Nakai J, 2012. Genetically encoded green fluorescent Ca^{2+} indicators with improved detectability for neuronal Ca^{2+} signals. PLoS One 7 (12), e51286. [PubMed: 23240011]

Patani R, Hardingham GE, Liddelow SA, 2023. Functional roles of reactive astrocytes in neuroinflammation and neurodegeneration. Nat. Rev. Neurol 19 (7), 395–409. 10.1038/s41582-023-00822-1. [PubMed: 37308616]

Perea G, Araque A, 2005. Properties of synaptically evoked astrocyte calcium signal reveal synaptic information processing by astrocytes. J. Neurosci 25 (9), 2192–2203. 10.1523/JNEUROSCI.3965-04.2005. [PubMed: 15745945]

Pirttimaki TM, Sims RE, Saunders G, Antonio SA, Codadu NK, Parri HR, 2017. Astrocyte-mediated neuronal synchronization properties revealed by false gliotransmitter release. J. Neurosci 37 (41), 9859–9870. 10.1523/JNEUROSCI.2761-16.2017. [PubMed: 28899919]

Pitt D, Werner P, Raine CS, 2000. Glutamate excitotoxicity in a model of multiple sclerosis. Nat. Med 6 (1), 67–70. 10.1038/71555. [PubMed: 10613826]

Ponath G, Park C, Pitt D, 2018. The role of astrocytes in multiple sclerosis. Front. Immunol 9, 217. 10.3389/fimmu.2018.00217. [PubMed: 29515568]

Potter LE, Paylor JW, Suh JS, Tenorio G, Caliaperumal J, Colbourne F, Baker G, Winship I, Kerr BJ, 2016. Altered excitatory-inhibitory balance within somatosensory cortex is associated with enhanced plasticity and pain sensitivity in a mouse model of multiple sclerosis. J. Neuroinflammation 13 (1), 142. 10.1186/s12974-016-0609-4. [PubMed: 27282914]

Robin LM, Oliveira da Cruz JF, Langlais VC, Martin-Fernandez M, Metna-Laurent M, Busquets-Garcia A, Bellocchio L, Soria-Gomez E, Papouin T, Varilh M, Sherwood MW, Belluomo I, Balcells G, Matias I, Bosier B, Drago F, Van Eeckhaut A, Smolders I, Georges F, Araque A, Panatier A, Oliet SHR, Marsicano G, 2018. Astroglial CB_1 receptors determine synaptic D-Serine availability to enable recognition memory. Neuron 98 (5), 935–944.e935. 10.1016/j.neuron.2018.04.034. [PubMed: 29779943]

Roth BL, 2016. DREADDs for Neuroscientists. Neuron 89 (4), 683–694. 10.1016/j.neuron.2016.01.040. [PubMed: 26889809]

Rothstein JD, Martin L, Levey AI, Dykes-Hoberg M, Jin L, Wu D, Nash N, Kuncl RW, 1994. Localization of neuronal and glial glutamate transporters. Neuron 13 (3), 713–725. 10.1016/0896-6273(94)90038-8. [PubMed: 7917301]

Rusakov DA, 2015. Disentangling calcium-driven astrocyte physiology. Nat. Rev. Neurosci 16, 226–233. 10.1038/nrn3878. [PubMed: 25757560]

Schindelin J, Arganda-Carreras I, Frise E, Kaynig V, Longair M, Pietzsch T, Preibisch S, Rueden C, Saalfeld S, Schmid B, Tinevez JY, White DJ, Hartenstein V, Eliceiri K, Tomancak P, Cardona A, 2012. Fiji: an open-source platform for biological-image analysis. Nat. Methods 9 (7), 676–682. 10.1038/nmeth.2019. [PubMed: 22743772]

Serrat R, Covelo A, Kouskoff V, Delcasso S, Ruiz-Calvo A, Chenouard N, Stella C, Blancard C, Salin B, Julio-Kalajzić F, Cannich A, Massa F, Varilh M, Deforges S, Robin LM, De Stefani D, Busquets-Garcia A, Gambino F, Beyeler A, Pouvreau S, Marsicano G, 2021. Astroglial ER-mitochondria calcium transfer mediates endocannabinoid-dependent synaptic integration. Cell Rep. 37 (12), 110133 10.1016/j.celrep.2021.110133. [PubMed: 34936875]

Shah D, Gsell W, Wahis J, Luckett ES, Jamoulle T, Vermaercke B, Preman P, Moechars D, Hendrickx V, Jaspers T, Craessaerts K, Horré K, Wolfs L, Fiers M, Holt M, Thal DR, Callaerts-Vegh Z, D'Hooge R, Vandenberghe R, Himmelreich U, Bonin V, De Strooper B, 2022. Astrocyte calcium dysfunction causes early network hyperactivity in Alzheimer's disease. Cell Rep. 40 (8), 111280 10.1016/j.celrep.2022.111280. [PubMed: 36001964]

Shigetomi E, Patel S, Khakh BS, 2016. Probing the complexities of astrocyte calcium signaling. Trends Cell Biol. 26 (4), 300–312. 10.1016/j.tcb.2016.01.003. [PubMed: 26896246]

Sofroniew MV, 2020. Astrocyte reactivity: subtypes, states, and functions in CNS innate immunity. Trends Immunol. 41 (9), 758–770. 10.1016/j.it.2020.07.004. [PubMed: 32819810]

Sun W, McConnell E, Pare JF, Xu Q, Chen M, Peng W, Lovatt D, Han X, Smith Y, Nedergaard M, 2013. Glutamate-dependent neuroglial calcium signaling differs between young and adult brain. Science 339 (6116), 197–200. 10.1126/science.1226740. [PubMed: 23307741]

Talantova M, Sanz-Blasco S, Zhang X, Xia P, Akhtar MW, Okamoto S, Dziewczapolski G, Nakamura T, Cao G, Pratt AE, Kang YJ, Tu S, Molokanova E, McKercher SR, Hires SA, Sason H, Stouffer DG, Buczynski MW, Solomon JP, Michael S, Powers ET, Kelly JW, Roberts A, Tong G, Fang-Newmeyer T, Parker J, Holland EA, Zhang D, Nakanishi N, Chen HS, Wolosker H, Wang Y, Parsons LH, Ambasudhan R, Masliah E, Heinemann SF, Piña-Crespo JC, Lipton SA, 2013. Aβ induces astrocytic glutamate release, extrasynaptic NMDA receptor activation, and synaptic loss. PNAS 110 (27), E2518–E2527. 10.1073/pnas.1306832110. [PubMed: 23776240]

Volterra A, Liaudet N, Savtchouk I, 2014. Astrocyte Ca^{2+} signalling: an unexpected complexity. Nat. Rev. Neurosci 15, 327–335. 10.1038/nrn3725. [PubMed: 24739787]

Walton C, King R, Rechtman L, Kaye W, Leray E, Marrie RA, Robertson N, La Rocca N, Uitdehaag B, van der Mei I, Wallin M, Helme A, Angood Napier C, Rijke N, Baneke P, 2020. Rising prevalence of multiple sclerosis worldwide: Insights from the Atlas of MS, third edition. Mult Scler 26, 1816–1821.4.e2259. 10.1016/j.neuron.2021.05.023. [PubMed: 33174475]

Wang X, Lou N, Xu Q, Tian GF, Peng WG, Han X, Kang J, Takano T, Nedergaard M, 2006. Astrocytic Ca^{2+} signaling evoked by sensory stimulation in vivo. Nat. Neurosci 9 (6), 816–823. 10.1038/nn1703. [PubMed: 16699507]

Yang G, Parkhurst CN, Hayes S, Gan WB, 2013. Peripheral elevation of TNF-α leads to early synaptic abnormalities in the mouse somatosensory cortex in experimental autoimmune encephalomyelitis. PNAS 110, 10306–10311. 10.1073/pnas.1222895110. [PubMed: 23733958]

Yu X, Nagai J, Khakh BS, 2020. Improved tools to study astrocytes. Nat. Rev. Neurosci 21, 121–138. 10.1038/s41583-020-0264-8. [PubMed: 32042146]

Ziehn MO, Avedisian AA, Tiwari-Woodruff S, Voskuhl RR, 2010. Hippocampal CA1 atrophy and synaptic loss during experimental autoimmune encephalomyelitis, EAE. Lab. Invest 90, 774–786. 10.1038/labinvest.2010.6. [PubMed: 20157291]

Zur Nieden R, Deitmer JW, 2006. The role of metabotropic glutamate receptors for the generation of calcium oscillations in rat hippocampal astrocytes in situ. Cereb. Cortex 16 (5), 676–687. 10.1093/cercor/bhj013. [PubMed: 16079243]

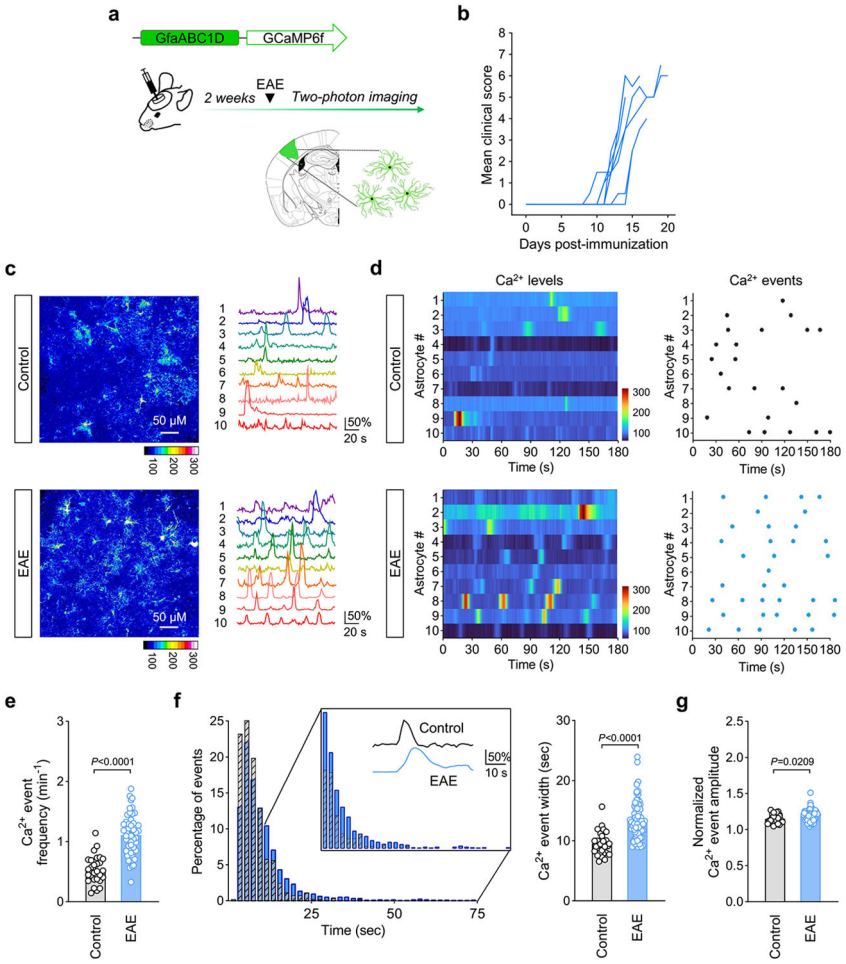

Fig. 1.

Spontaneous hyperactivity of cortical astrocytes during EAE. (**a**) Experimental approach for *ex vivo* recording of astrocytic calcium activity in the mouse somatosensory cortex during EAE. Two-photon imaging was performed in cortical slices from control and EAE mice injected with GFAP-GCaMP6f viral particles. (**b**) Neurological score mice included in the analysis of spontaneous calcium activity in cortical astrocytes (13–20 dpi). (**c**) Representative images and individual traces of astrocyte calcium events accumulated over a 3 min period in acute cortical slices from control (top) and EAE (bottom) mice. (**d**) Heat maps and raster plots depicting calcium levels and spontaneous events along time in control and EAE astrocytes. (**e-g**) Analysis of calcium event frequency, duration and amplitude in cortical astrocytes from control (28 slices, 5 mice) and EAE (53 slices, 8 mice) conditions. (**f**) *Left*: Representative histogram showing the percentage of astrocyte calcium events and their duration in control and immunized mice. Box: percentages of events with longer duration in EAE mice and representative traces from control (gray) and EAE (blue) astrocytes. *Right*: width of calcium events in cortical astrocytes from naïve and immunized mice. Data were analyzed with unpaired *t* test or Mann-Whitney test. Error bars express SEM.

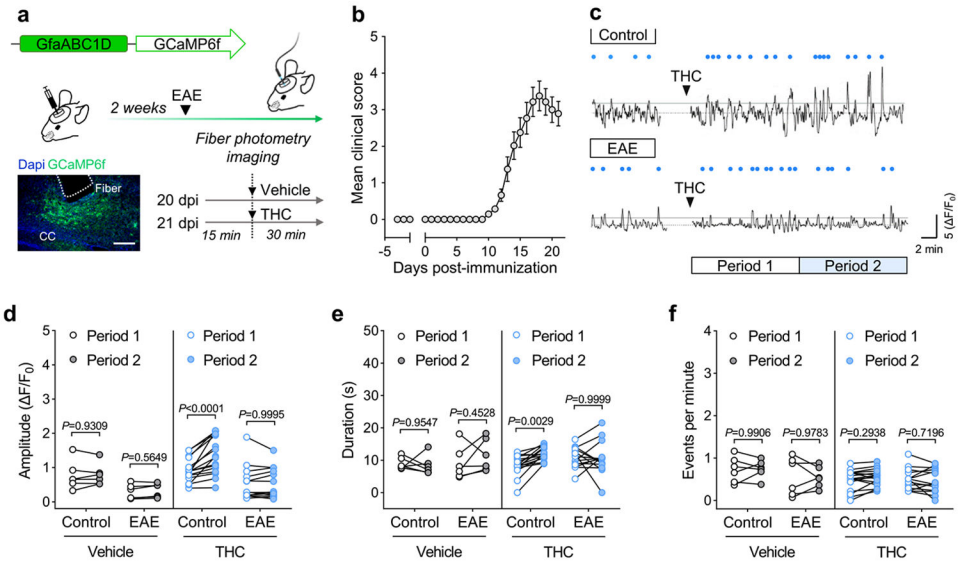

Fig. 2.

EAE impairs CB_1 receptor-mediated astrocyte calcium responses. (**a**) Fiber photometry approach for *in vivo* recording of astrocytic calcium responses to THC in EAE mice. Fiber photometry imaging was performed in control and EAE mice on 2 independent recording sessions at 20 dpi (vehicle) and 21 dpi (THC). *Below*: representative image of GCaMP6s expression in the somatosensory cortex. DAPI is marked in blue and GCaMP6s in green. Scale bar: 200 μm. (**b**) Neurological score of EAE mice included in the study (14 mice; 3 independent EAE experiments). (**c**) Representative recordings from the mouse somatosensory cortex showing the effect of THC (10 mg/Kg; i.p.) on astrocytic calcium activity in control (top) and EAE (bottom) mice. Blue dots correspond to detected transients above the threshold (median + 2*MAD) in mice injected with vehicle and THC. White and blue rectangles show the time window of analyzed *period 1* and *period 2*, respectively. The first minute before and after injection was removed to exclude mouse-handling/injection effects. (**d**–**f**) Quantitative analysis of astrocyte calcium responses to vehicle and THC in control and EAE mice (6–16 mice per experimental group). Data were analyzed by two-way ANOVA followed by Šídák's multiple comparisons test.

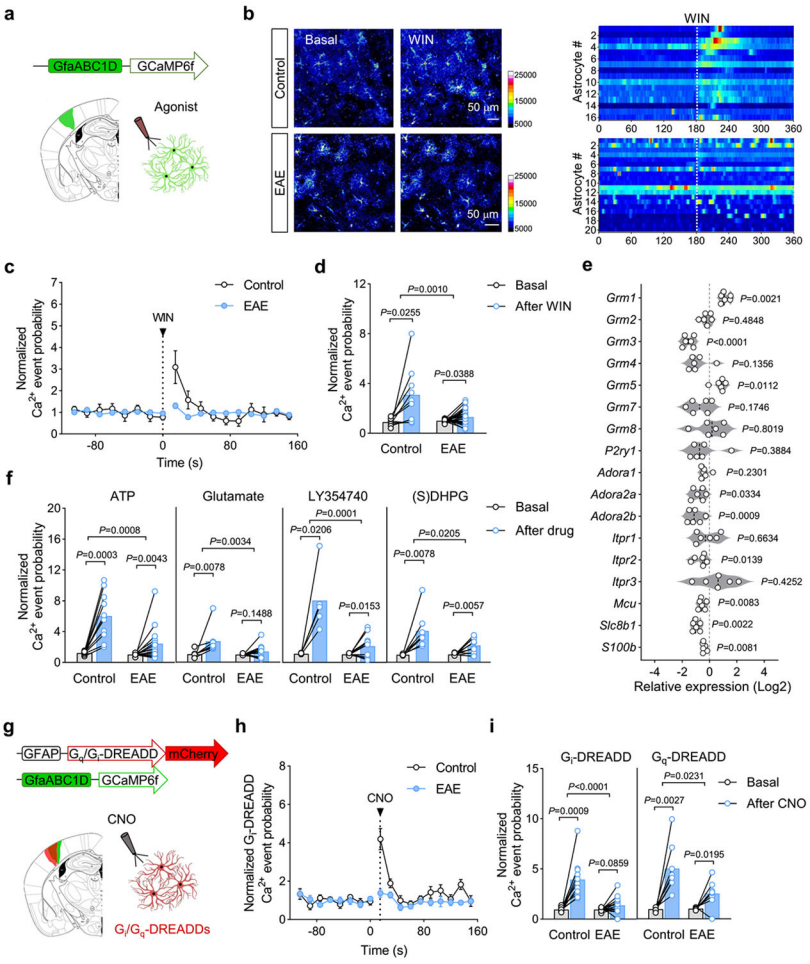

Fig. 3.

Cell autonomous deregulation of astrocyte calcium signaling pathways during EAE. (**a**) *Ex vivo* analysis of neurotransmitter receptor-mediated astrocyte calcium responses during EAE. Agonists were applied locally to the somatosensory cortex in acute slices from mice injected with the AAV vector encoding for GCaMP6f under the Gfa-ABC1D promoter. (**b**) *Left*: pseudocolor images obtained from cortical astrocytes of control (top) and EAE (bottom) mice before and after local application of the CB_1 receptor agonist WIN55,212-2 (WIN; 300 µM). *Right*: heat map depicting calcium levels along time following application of the cannabinoid agonist in control and EAE astrocytes. (**c**) Normalized astrocyte calcium event probability over time showing the effect of WIN in control and immunized mice. (**d**) Bar graph depicting calcium event probability normalized to basal activity before and after WIN application in control (9 slices, 5 mice) and EAE astrocytes (25 slices, 7 mice). The dotted lines in **b** and **c** indicate 5 sec of WIN application. Data were analyzed by two-tailed paired Student's *t* test (before and after) and unpaired *t* test or Mann-Whitney test (between groups). (**e**) Expression levels of calcium handling genes in astrocytes purified at acute EAE disease relative to those in healthy controls. Data were analyzed by two-tailed unpaired Student's *t* test or Mann-Whitney test. (**f**) Calcium event probability normalized to basal activity before and after application of ATP (200 µM; 11–15 slices, 5–7 mice), glutamate

(200 μM; 8–13 slices, 4–6 mice), LY354740 (100 μM; 5–14 slices, 2–2 mice) and (S)DHPG (100 μM; 8–10 slices, 2–2 mice) in control and EAE astrocytes. Data were analyzed by two-tailed paired Student's *t* test (before and after) and unpaired *t* test or Mann-Whitney test (between groups). (**g**) *Ex vivo* analysis of G_i and G_q mediated signaling on astrocyte calcium responses during EAE. Clozapine-N-oxide (CNO, 1 mM) was applied locally in acute cortical slices from mice injected with AAV vectors encoding for GCaMP6f and for G_i- or G_q-DREADDs under the astrocyte promoters GFAP or GfaABC1D. (**h**) Calcium event probability normalized to basal activity over time before and after CNO application in control and EAE mice injected with AAV5-GFAP-G_i-DREADD-mCherry. The dotted line indicates 5 sec of CNO application. (**i**) Normalized calcium event before and after CNO application in control and EAE astrocytes expressing G_i-DREADDs (11–15 slices; 2–4 mice) or G_q-DREADDs (8–9 slices, 3–3 mice). Data were analyzed by two-tailed Student's paired *t* test (before and after) and unpaired *t* test or Mann-Whitney test (between groups). Error bars express SEM.

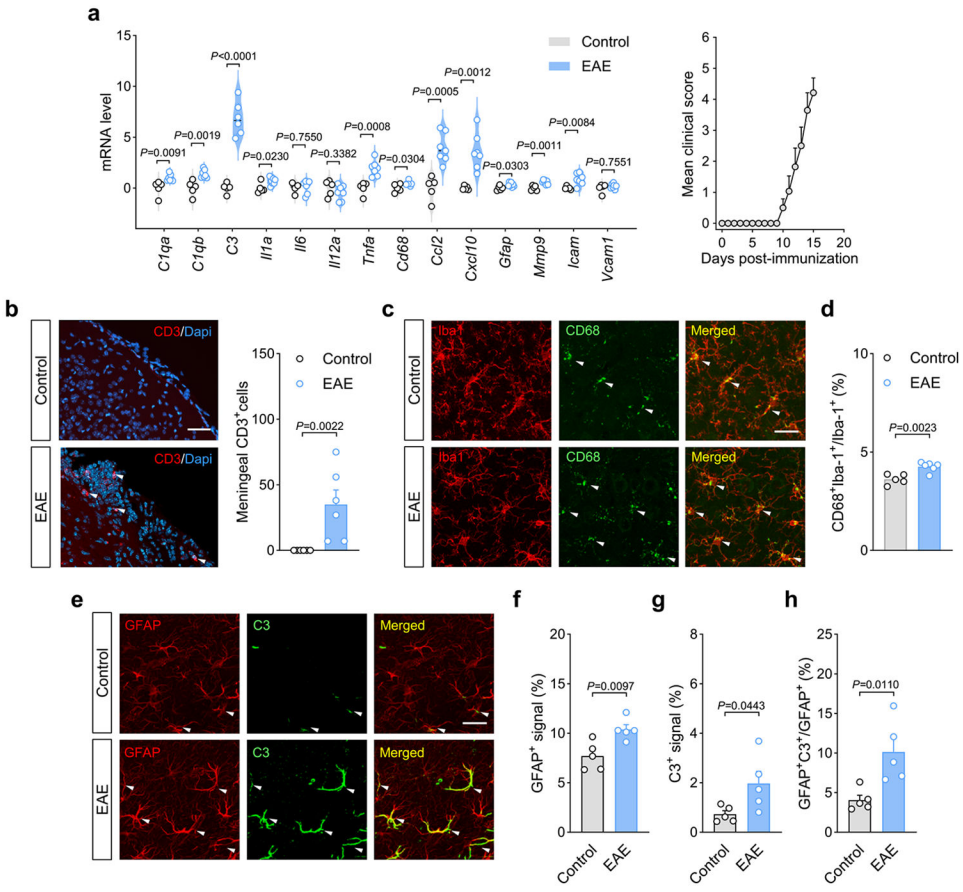

Fig. 4.

Local inflammation in the cortex of EAE mice. (**a**) Gene expression analysis of pro-inflammatory mediators and inflammatory markers in the somatosensory cortex of EAE mice at acute disease (16 dpi; 7 mice) relative to those in control animals (5 mice). The mean clinical score of EAE mice included in the analysis is depicted on the *right panel*. Data were analyzed by two-tailed paired Student's *t* test or Mann-Whitney test. (**b**) Representative images and quantitative analysis of meningeal $CD3^+$ immunopositive T cells in coronal sections of EAE (14 dpi; 6 mice) and control conditions (5 mice) Scale bar = 50 μm. Data were analyzed by two-tailed Mann-Whitney test. (**c**) Representative confocal images showing the distribution of CD68 immunopositive puncta and Iba1-positive microglia in layer VI of the somatosensory cortex from control and EAE mice (17 dpi). Scale bar = 25 μm. (**d**) Quantification of CD68 levels within Iba1-positive profiles indicate microglia activation the EAE cortex (5–6 mice). Data were analyzed by two-tailed unpaired Student *t* test. (**e**) Representative confocal micrographs depict immunolabeling of the astrocyte reactivity marker GFAP and complement component 3 (C3) in layer VI from control and EAE conditions. Scale bar = 25 μm. (**f**–**h**) Quantitative analysis of GFAP (**f**) and C3 (**g**) levels and C3 expression in astroglial profiles (**h**) shows augmented astrocyte reactivity in the EAE cortex. Data were analyzed by two-tailed unpaired Student *t* test. Error bars express SEM.

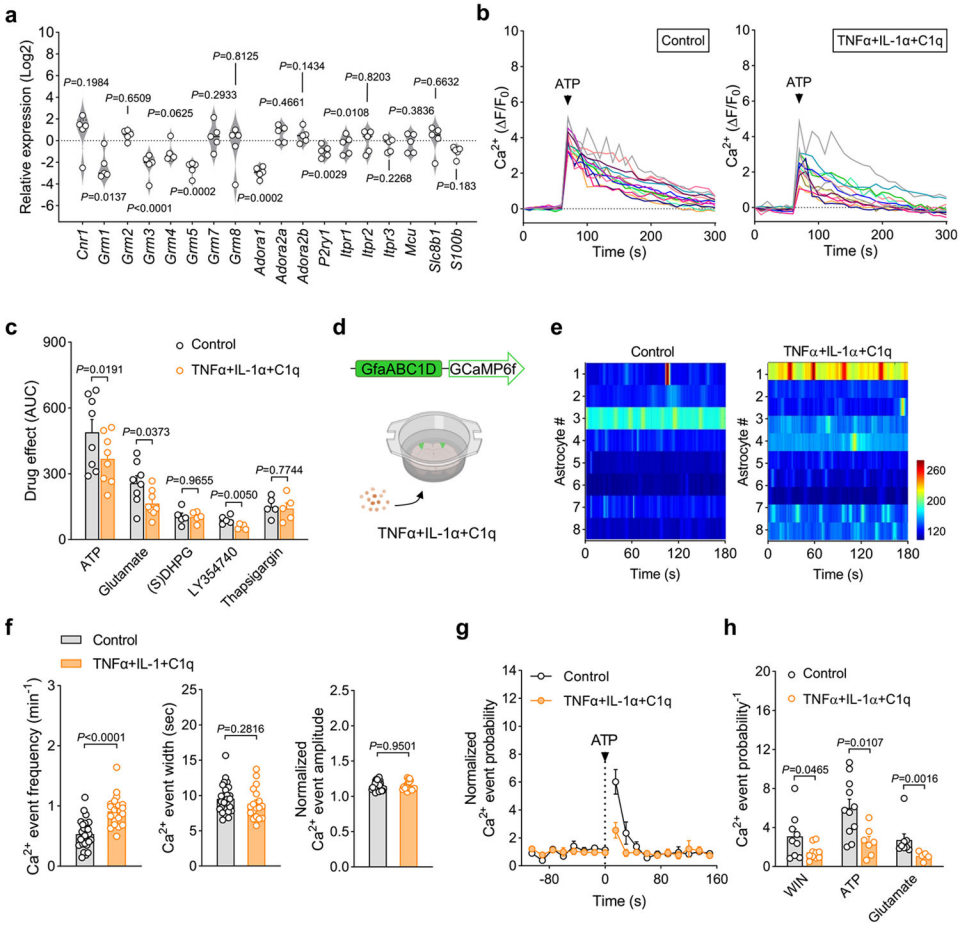

Fig. 5.

Pro-inflammatory signals engage aberrant astrocyte calcium activity. (**a**) Gene expression analysis of astrocyte calcium handling molecules in cultured cells activated *in vitro* by incubation with the pro-inflammatory factors TNFα (25 ng/ml), IL-1α (3 ng/ml) and C1q (400 ng/ml) (18–24 h). Data were analyzed by two-tailed paired Student's *t* test or Mann-Whitney test. (**b**) Representative imaging experiments showing calcium responses of individual astrocytes evoked by *in vitro* exposure to ATP (200 μM). (**c**) Quantitative analysis of calcium responses by ATP (200 μM), glutamate (200 μM), (S) DHPG (200 μM), LY354740 (200 μM), ATP (200 μM) and thapsigargin (1 μM) in astrocyte cultures incubated with TNFα + IL-1α + C1q. AUC, area under the curve. Data were analyzed by two-tailed paired Student's *t* test or Mann-Whitney test. (**d**) *Ex vivo* analysis of astrocyte calcium dynamics in response to pro-inflammatory factors. Acute cortical slices from mice injected with the AAV vector encoding for GCaMP6f under the Gfa-ABC1D promoter were imaged following incubation with TNFα + IL-1α C1q (30 min). (**e**) Heat maps showing astrocytic calcium levels of individual astrocytes along time in cortical slices activated *ex vivo* with TNFα + IL-1α + C1q. (**f**) Frequency, duration and amplitude of spontaneous astrocyte calcium events in control conditions (28 slices, 5 mice) and following activation with pro-inflammatory factors (22 slices, 4 mice). Data were analyzed by two-tailed unpaired Student's *t* test. (**g**) Calcium event probability normalized to basal activity over time

depicting the effect of ATP (200 μM) in cortical astrocytes activated *ex vivo* with TNFα + IL-1α + C1q. (**h**) Calcium event probability normalized to basal activity depicting the effect of WIN55,212–2 (WIN; 300 μM), ATP (200 μM) or glutamate (200 μM) in control astrocytes (8–11 slices, 5 mice) and following incubation with pro-inflammatory factors (5–10 slices, 4 mice). Data were analyzed by two-tailed paired Student's *t* test (before and after). Error bars express SEM.

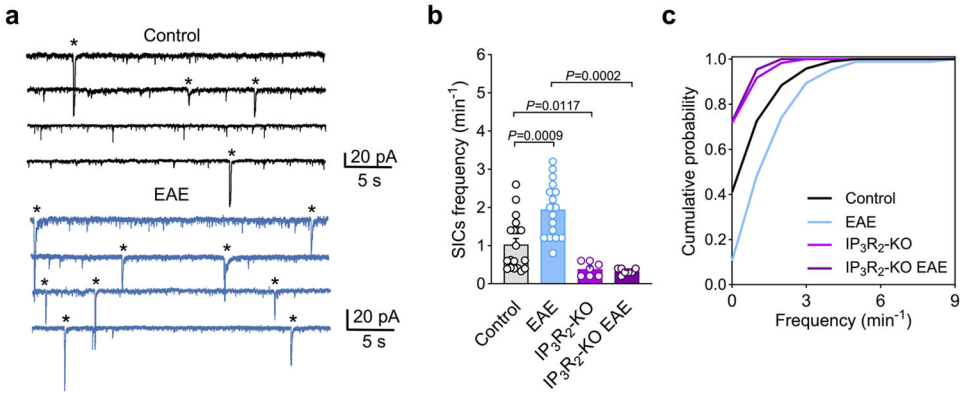

Fig. 6.

Exacerbated astrocytic glutamate release in the EAE cortex. (**a**) Representative traces depicting slow inward currents (SICs) (asterisks) in layer V pyramidal neurons within the somatosensory cortex from control and EAE mice. (**b**) Frequency of SICs in control (19 neurons, 4 mice), EAE (17 neurons, 6 mice), IP_3R_2-KO (7 neurons, 2 mice) and IP_3R_2-KO EAE (7 neurons, 2 mice) animals. Data were analyzed by one-way ANOVA followed by a Dunn's test for multiple comparisons. Error bars express SEM. (**c**) Cumulative frequency of SICs in cortical neurons from wild-type and IP_3R_2-KO mice in control and EAE conditions.

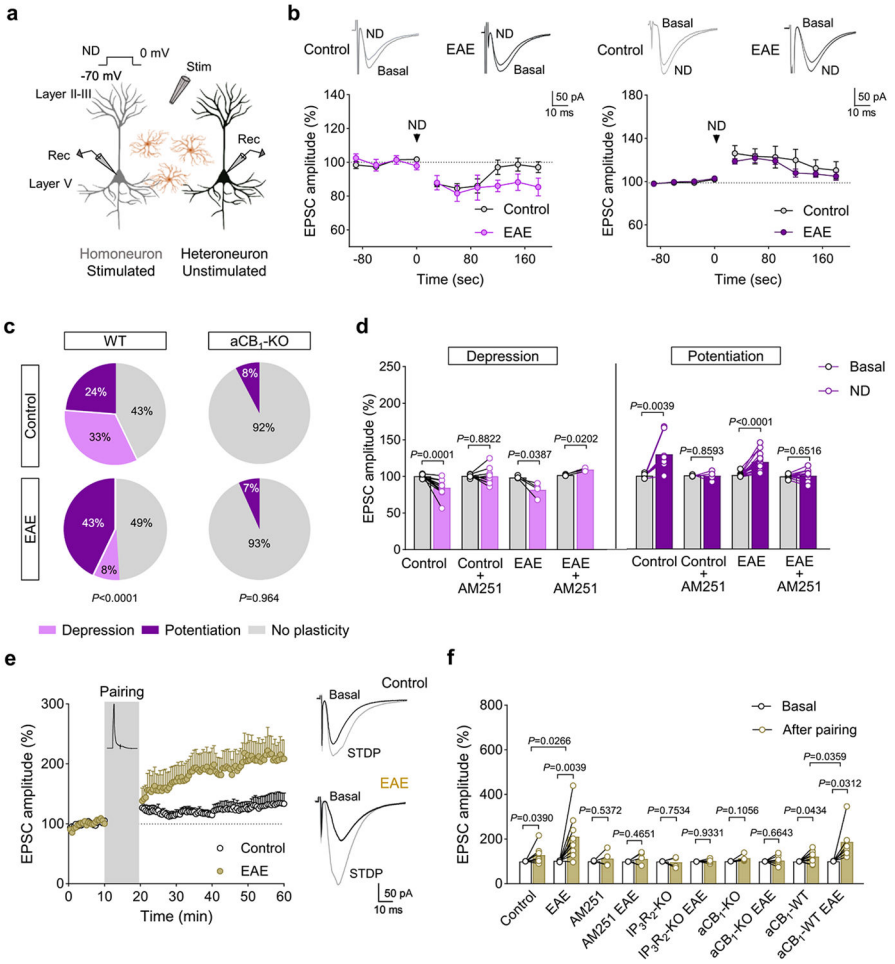

Fig. 7.

EAE disrupts astrocyte-mediated cortical neuron network plasticity. (**a**) Double patch-recordings from layer V pyramidal neurons in the somatosensory cortex for the analysis of astrocyte-neuron communication. (**b**) Time-courses and representative EPSC traces show heteroneuronal depression (**b**, *left panel*) and potentiation (**b**, *right panel*) of synaptic transmission following homoneuronal depolarization (ND) in control and EAE mice. (**c**) Percentages of heteroneurons that showed depression, potentiation or no plasticity in wild-type (WT) mice (control, 42 pairs, 7 mice; EAE, 49 pairs, 9 mice; $P < 0.0001$) and $CB_1^{f/f}$ mice injected with AAV9-GFAP-Cre in the somatosensory cortex (aCB_1-KO) (control, 13 pairs, 2 mice; EAE, 15 pairs, 2 mice; $P = 0.9646$). Data were analyzed by Chi-square test. (**d**) Relative changes in EPSC amplitude depict heteroneuronal depression and potentiation in control (14 and 10 pairs, 6–5 mice), AM251 (2 μM) (9 and 4 pairs, 5–4 mice), EAE (4 and 21 pairs, 3–8 mice), EAE+AM251 (3 and 12 pairs, 2–8 mice) conditions. Data were analyzed by two-tailed paired Student *t* test. (**e**) Time-course of EPSC amplitude in layer V pyramidal neurons depicts spike-timing dependent plasticity (STDP) induced in control and EAE mice by pairing a postsynaptically evoked action potential with an EPSP (Δt = −25 ms) 60 times in 10 min (gray area). (**f**) Relative changes in EPSC amplitude after the pairing period in control and immunized mice (8 and 10 neurons, 4–7 mice), in the

presence of AM251 (4 and 5 neurons, 2–3 mice), in IP_3R_2-KO animals (4 and 4 neurons, 2–2 mice), and in aCB_1-KO (5–7 neurons, 2–3 mice) or aCB_1-WT (9 and 6 neurons, 3–3 mice) mice injected with AAV9-GFAP-Cre and AAV9-GFAP-mCherry, respectively. Data were analyzed by two-tailed paired Student's *t* test or Wilcoxon test (before and after) and Mann-Whitney test (between groups). Error bars express SEM.